

*Chapter 1*

## REAL-TIME FATIGUE DAMAGE MONITORING VIA IN SITU ULTRASONIC SENSING\*

*Shalabh Gupta<sup>†</sup> and Asok Ray<sup>‡</sup>*

Mechanical Engineering Department, The Pennsylvania State University  
University Park, PA 16802, USA

### Abstract

Estimation of structural damage and quantification of structural integrity are critical for safe and reliable operation of human-engineered complex systems. Fatigue damage is one of the most commonly encountered sources of structural degradation in mechanical systems. Detection of incipient fatigue damage is essential for averting widespread crack growth that leads to catastrophic failures.

This chapter presents online in situ monitoring of fatigue damage using the ultrasonic sensing technique that is sensitive to small microstructural changes, robust to measurement noise, and also suitable for real-time applications. A recently reported information-theoretic method of data-driven pattern recognition, called Symbolic Dynamic Filtering (*SDF*), has been used for real-time analysis of ultrasonic data, where the time series data in the fast scale of process dynamics are analyzed at discrete epochs in the slow scale of fatigue damage evolution. *SDF* includes pre-processing of ultrasonic data using wavelet transform, which is well suited for time-frequency analysis of non-stationary signals and enables noise attenuation in raw data. The wavelet-transformed data is partitioned using the maximum entropy principle to generate symbol sequences, such that the regions of data space with more information are partitioned finer and those with sparse information are partitioned coarser. Subsequently, statistical patterns of evolving damage are identified from these sequences by construction of a (probabilistic) finite-state machine that captures the dynamical system behavior by information compression.

A computer-controlled fatigue test apparatus, equipped with ultrasonic sensors and an optical microscope, has been used to experimentally validate the concept of ultrasonic based real-time monitoring of fatigue damage in polycrystalline alloys. The task

---

\*This work has been supported in part by the U.S. Army Research laboratory and the U.S. Army Research Office under Grant No. DAAD19-01-1-0646.

<sup>†</sup>E-mail address: szg107@psu.edu

<sup>‡</sup>E-mail address: axr2@psu.edu

of fatigue damage monitoring is formulated as: (i) forward problem of pattern recognition for (offline) characterization of the statistical behavior of fatigue damage evolution and (ii) inverse problem of pattern identification for (online) estimation of the remaining useful life based on the real time ultrasonic data and the statistical information generated offline.

## 1. Introduction

Gradually evolving changes in the structural parameters of a mechanical system over its service life may generate uncertainties in both transient and stationary behavior. This problem is often addressed by overly conservative estimates of the design parameters due to lack of available information. Consequently, the engineering design of mechanical systems suffers from enforcement of large safety factors and results in manufacture of cumbersome and unnecessarily expensive machinery. The alternative is to have expensive and time-consuming inspections. In the current state-of-the-art maintenance actions are based on fixed usage intervals. On-line sensing of damage would allow re-evaluation and extension of service life and inherent protection against unforeseen early failures to reduce the frequency of inspections and increase the mean time between major maintenance actions on serviceable structures.

Prediction of structural damage and quantification of structural integrity are critical for safe and reliable operation of human-engineered complex systems. Fatigue damage is one of the most commonly encountered sources of structural degradation during both nominal and off-nominal operations of such systems [1]. Detection of fatigue damage at an early stage is essential because the accumulated damage could potentially cause catastrophic failures in the system, leading to loss of expensive equipment and human life [1]. Therefore, it is necessary to develop diagnosis and prognosis capabilities for reliable and safe operation of the system and for enhanced availability of its service life. In the current state-of-the-art, direct measurements of fatigue damage at an early stage (e.g., crack initiation) are not feasible due to lack of appropriate sensing devices and analytical models. This chapter attempts to address this inadequacy by taking advantage of the sensitivity of the ultrasonic impedance on small changes that occur inside the material during the early stages of fatigue damage [2]. Since a vast majority of structural components that are prone to fatigue damage are made of ductile alloys, this chapter dwells on fatigue damage sensing and prediction for such materials.

Sole reliance on model-based analysis for structural damage monitoring is infeasible because of the difficulty in achieving requisite accuracy in modeling of fatigue damage evolution. Many model-based techniques have been reported in recent literature for structural health monitoring, remaining life estimation and prediction of damage precursors [3][4][5][6][7][8]. Apparently, no existing model, solely based on the basic fundamental principles of physics [9], can adequately capture the dynamical behavior of fatigue damage at the grain level. In general, these models are critically dependent on the initial defects in the materials, which may randomly form crack nucleation sites and identification of exact initial and boundary conditions is not feasible. As such, these defects are difficult to identify and model [10][11].

Small deviations in the distribution of initial defects may produce large variations in the

evolution of fatigue damage for (apparently) identical specimens under the same loading and environmental conditions [11]. Specifically in the short crack region the appearance of many crack nucleation sites can be treated as random events. This random distribution of micro-structural flaws produce a wide uncertainty in the crack initiation phase [1][11]. For example, inclusions, casting defects and machining marks originating during fabrication may cause stress augmentation at certain locations. These surface and sub-surface defects that are largely unavoidable constitute integral parts of the material microstructure of the operating machinery. In addition, fluctuations in usage patterns (e.g., random overloads) and environmental conditions (e.g., temperature and humidity) may adversely affect the performance and service life of mechanical systems leading to unanticipated failures. As such, evolution of fatigue damage is considered as a stochastic phenomenon [1][11][12]. A stochastic measure of fatigue crack growth is proposed in recent literature [13].

The stochastic phenomenon of fatigue damage evolution makes the maintenance efforts more conservative, difficult and expensive. With heavy usage and stringent safety requirements, as the machinery ages, the frequency of major maintenance increases and leads to premature replacements of the critical components. However, in general, both safety and economics suffer as no good compromise can be achieved without systematic analysis of the situation. This problem motivates the research, since one of the most fundamental solutions to this problem is on-line failure diagnosis as well as on-line prognosis that allows remaining life prediction for the critical structural components of operating machinery, under anticipated load profiles.

The above discussion evinces the need for online updating of information using sensing devices (e.g., ultrasonics, acoustic emission and eddy currents) which are sensitive to small microstructural changes and can provide useful and reliable estimates of the anomalies at early stages of fatigue damage evolution [2]. This chapter presents real-time fatigue damage monitoring using the ultrasonic sensing technique to examine small microstructural changes in polycrystalline alloys during both fatigue crack initiation and propagation phases. Consequently, the analysis of time series data from available sensors is essential for monitoring the evolving fatigue damage in real time [14].

The theme of data-driven pattern recognition and anomaly detection, formulated in this chapter, is built upon the concepts of *Symbolic Dynamics* [15], *Finite State Automata* [16], *Statistical Mechanics* [17], and *Information Theory* as a means to qualitatively describe the dynamical behavior in terms of symbol sequences [18][19][20][15]. The chapter presents symbolic dynamic filtering (*SDF*) [18][21][17][22][23] to analyze time series data of sensors (e.g., ultrasonic) for detection and identification of gradually evolving fatigue damage.

To this end, a computer-controlled fatigue test apparatus, equipped with multiple sensing devices (e.g., ultrasonics and optical microscope), has been used to experimentally validate the concept of real-time fatigue damage monitoring. The sensor information is integrated with a software module consisting of the *SDF* algorithm for real-time monitoring of fatigue damage. Experiments have been conducted under different loading conditions on specimens constructed from the ductile aluminium alloy 7075 – T6.

This chapter is organized in eight sections and one appendix. Section 1. provides a brief discussion of the problem statement of real-time fatigue damage monitoring using sensing devices such as the ultrasonics. Section 2. provides the background of fatigue damage sensing methods and motivation of the current research. Section 3. presents the details of

experimental apparatus used for validating the concept of real-time fatigue damage monitoring. Section 4. formulates the problem of fatigue damage monitoring in the setting of two-time-scales and briefly describes the procedure of a recently reported data-driven pattern recognition tool, called symbolic dynamic filtering (*SDF*). Section 5. provides an overview of the forward and the inverse problems of anomaly detection in complex dynamical systems. Section 6. presents the details of experimental procedure, *SDF*-based pattern recognition and results of real-time fatigue damage detection using ultrasonic sensing technology. Section 7. presents the solution procedure and results derived from both the forward and the inverse problems for real-time fatigue damage estimation. Section 8. summarizes and concludes the chapter with recommendations for future research. Appendix Appendix A. provides a brief overview of symbolic dynamic filtering (*SDF*) including the concepts of symbolic dynamic encoding, wavelet based partitioning, probabilistic finite state machine construction and pattern identification.

## 2. Fatigue Damage Sensing Techniques

Several techniques based on different sensing devices (e.g., ultrasonics, acoustic emission and eddy currents) have been proposed in recent literature for fatigue crack monitoring [24][25][26]. The capabilities of electrochemical sensors [27] and thermal imaging techniques [28] have also been investigated for structural failure analysis. A review of different vibration based damage detection and identification methods is provided by Doebling et. al [29]. This section presents a brief review of fatigue damage sensing methods as below.

### 2.1. Acoustic Emission

Acoustic emissions are the stress waves that are produced due to sudden redistribution of the stress inside the material structure. Some of the possible causes of the changes in the internal structure of the material can be dislocation movement, crack initiation and growth, and crack opening and closure. Since the primary sources of acoustic emissions are damage-related, the detection and monitoring of these emissions are commonly used to predict and estimate material failure. As such, acoustic emission technique is commonly used to monitor defects and causes of failures in structural materials. This technique has been employed and tested for fault diagnosis in numerous applications including polycrystalline alloys, composite materials, and also in the study of mechanical behavior of ceramics and rocks. The traditional analysis methods using acoustic emission technique include monitoring the acoustic-emission counts, the peak levels, and the energy of the signal. These parameters are used for correlation with the defect formation mechanisms and for providing a quantified estimate of faults.

Acoustic emission technique has been investigated by several researchers for early detection of fatigue and fracture failures of materials [30][31][32][33][34][35][36]. Acoustic emission technique has also been widely used for detection of faults or leakage in pressure vessels, tanks, and piping systems and for monitoring the welding and corrosion progress in materials. One of the advantages here is that acoustic emissions are sensitive to the activities occurring inside the material microstructure. Moreover, acoustic emission sensors are compact and can be easily mounted on the surface of a specimen being examined for online

testing and for continuous monitoring of evolving damage. The major drawback of acoustic emission technique is that the acoustic emission signals are usually very weak and give poor performance in noisy environments where signal-noise separation becomes a difficult task.

## 2.2. Eddy Currents

The other common sensing technique used for fault diagnosis in structural materials is the eddy current technique that is based on the principal of electromagnetism. Eddy currents are produced through a process called electromagnetic induction. When a source of alternating current is supplied to a conducting material, such as a copper wire, a magnetic field develops in and around the material. Eddy currents are induced electrical currents that are produced in another electrical conductor that is brought into a close proximity of this magnetic field. The presence of a crack or detriment in the material affects the flow pattern of the eddy current, which can be detected for prediction and estimation of the structural damage [37][38][39]. The advantages of eddy current inspection technique include sensitivity to small cracks and other defects, portability of sensor equipment, minimum part preparation, and non-contact evaluation. However, there are certain limitations of the eddy current inspection technique such as the depth of penetration is limited, only conductive materials can be inspected, and surface finish and roughness may interfere. Since eddy currents tend to concentrate at the surface of a material, they can only be used to detect surface and near surface defects.

## 2.3. Ultrasonics

Another common method for fault diagnosis in structural materials is using the ultrasonic sensing technique. The ultrasonic flaw detector functions by emitting high frequency ultrasonic pulses that travel through the specimen and return back through the receiver transducers. As with the propagation of any wave, it is possible that discontinuities in the propagation media will cause additive and destructive interference. Since material characteristics (e.g., voids, dislocations and short cracks) influence the ultrasonic impedance, a small fault in the specimen is likely to change the signature of the signal at the receiver end. Therefore, the signal can be used to capture some of the minute details and small changes during the early stages of fatigue damage, which may not be possible to detect by an optical microscope [2]. Ultrasonic sensing methodology has been effectively utilized for microstructural analysis in polycrystalline alloys to examine the fatigue phenomenon [40][41]. Impedance of the ultrasonic signals has been shown to be sensitive to small microstructural changes occurring during the early stages of fatigue damage [2][42][43][44]. Moreover, ultrasonic sensing is applicable to real-time applications and the sensing probes can be easily installed on the specimen. Ultrasonic sensing technique is also robust to noisy environments since the externally excited waves are of very high frequency and they do not interfere with small disturbances. As such, the research in this chapter is based on ultrasonic sensing technique to examine small microstructural changes during early stages of fatigue damage evolution [44][45][46].

### 3. Fatigue Damage Test Apparatus

This section presents the description of an experimental apparatus that is designed to study the growth of fatigue damage in mechanical systems [47]. The main content of this section include the description of the fatigue damage testing apparatus that is equipped with different sensing devices for process control and real-time monitoring of fatigue damage.

The primary objective of the fatigue test apparatus is to demonstrate online sensing and prediction of fatigue damage. As such, the requirements of the apparatus are:

- Capability to operate under cyclic loading with multiple sources of input excitation
- Provision of a failure site such that the damage accumulation takes place within a reasonable period of time in the laboratory environment with negligible damage to other components of the test apparatus
- Capability of real-time data acquisition from appropriate sensing devices
- Accommodation of online data analysis tools for monitoring the evolution of fatigue damage in real time.

The experimental apparatus, shown in Figure 1, is a special-purpose uniaxial fatigue testing machine that operates on the hydraulic power supplied by a hydraulic pump device, which moves under load control at speeds up to 12.5 Hz; a detailed description of the apparatus and its design specifications are reported in [47]. The test apparatus is also connected to three computers dedicated for the tasks of data acquisition and control. The test specimens are subjected to tensile-tensile cyclic loading by a hydraulic cylinder under the regulation of computer-controlled electro-hydraulic servo-valves.

The feedback signals that are generated from the load cell and the extensometer are processed by signal conditioners that include standard amplifiers and signal processing units. These signals are passed to the controller that governs the hydraulic servo-valve for operation under specified load and position limits. The image data of the specimen surface from the optical microscope and the sensor data from the ultrasonic transducers are passed to the data analysis and damage estimation subsystem. The information from the optical microscope is analyzed to determine the fatigue crack length on the specimen surface. Data sets from the ultrasonic sensors are analyzed using symbolic dynamic filtering (*SDF*) algorithm for fatigue damage estimation even before the optical microscope detects a surface crack.

A brief description of the associated computer hardware, process instrumentation and the control module of the fatigue test apparatus is provided below.

- *Subsystem for Closed Loop Servo-Hydraulic Unit and Controller:* The instrumentation and control of the computer-controlled uniaxial fatigue test apparatus includes a load cell, an extensometer, an actuator, the hydraulic system, and the controller. The servo-hydraulic unit can excite the system with either random loads or random strains at variable amplitudes. The control module is installed on a computer which is dedicated to machine operation. The controller operates the machine according to a schedule file that contains the specifications of the loading profile and the number

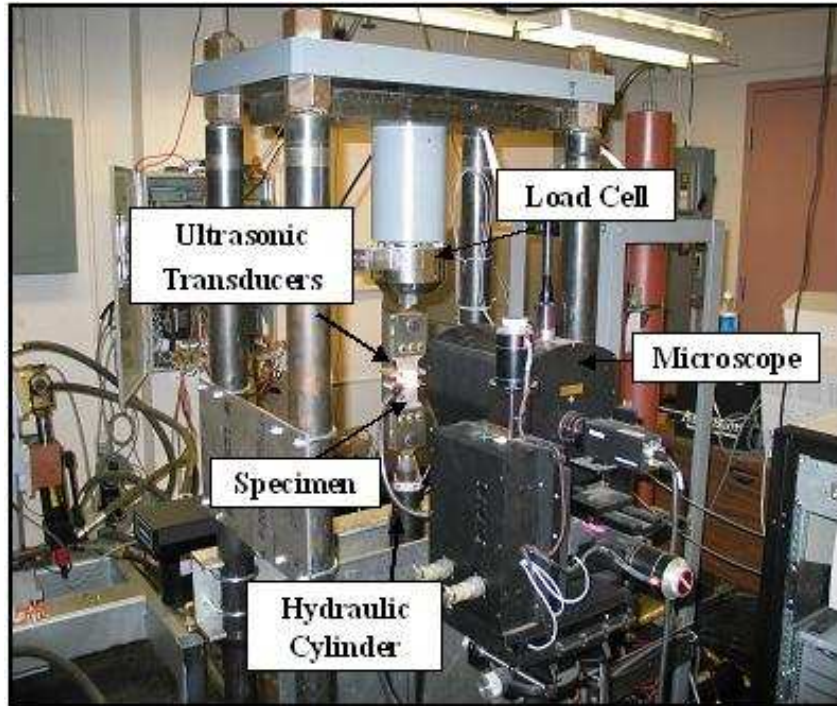


Figure 1. Fatigue Damage Test Apparatus.

of load cycles for each type of test in the profile. The real time data from the extensometer and the load cell are supplied to the controller for operation under specified position and load limits.

- *Subsystem for data acquisition, signal processing, and engineering analysis:* In addition to the computer for controlling the load frame, a second computer is used for real-time image data collection from the microscope to monitor the growth of surface cracks. The instrumentation for the ultrasonic flaw detection scheme is connected to a third computer. The real time ultrasonic data collected on this computer is transferred at regular intervals to a fourth computer on which the data analysis algorithm is installed. The algorithm based on symbolic dynamic filtering (*SDF*) generates the information about fatigue damage in terms of anomaly measures at different time epochs and the corresponding plots are displayed on the screen in real time. These laboratory computers are interconnected by a local dedicated network for data acquisition, data communications, and control. An Ethernet network and an *RS – 232* serial data line connect the computers.

The main elements of the hydraulic pump system are a 3-phase induction motor driven pump, the oil supply manifold, and the cylinder. The purpose of the supply manifold is to properly sequence the system pressure and to accommodate the accumulators. The accumulators maintain the system pressure when the instantaneous demand from the servo valve/cylinder is higher than the flow rate available from the pump. A small solenoid valve is used under most shutdown conditions to bleed the accumulator pressure slowly. This

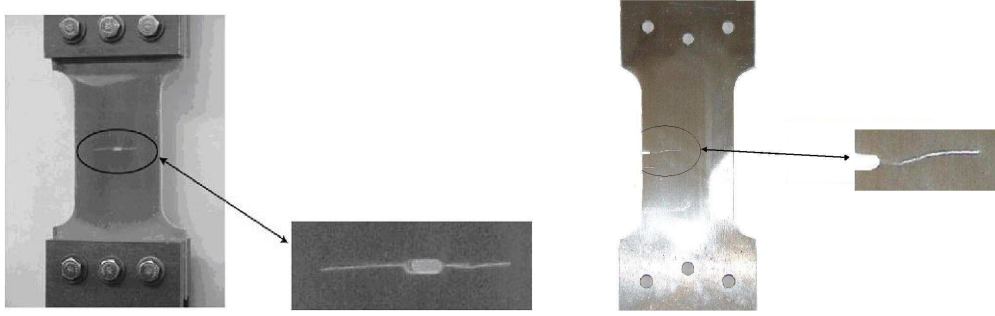


Figure 2. Cracked specimens: a) Left image- specimen with a center notch and b) Right image- specimen with a side notch.

prevents a high-pressure spike from causing the return filters to fail. The hydraulic cylinder has a 6 inch ( $\sim 152$  mm) bore and a 2.5 inch ( $\sim 64$  mm) stroke length, and is double ended (i.e., the rod extends through seals at both ends of the cylinder).

The software effectively has two threads of operation, the main program and the controller program. A detailed description of the software and the associated hardware is provided in [47]. The software programs for control and data acquisition are written in C++ programming language and are installed in the real-time Linux operating environment. The main program is *the user space* that enforces the test sequence. The controller is installed in *the kernel space* which is an Interrupt Service Routine (*ISR*) that generates the Direct Memory Access (*DMA*) completion interrupt signals. The analog-to-digital (*A/D*) board is initialized to take 20 readings per frame, which represents 10 readings each for 2 channels. These channels are connected to the load cell output and Linear Variable Differential Transformer (*LVDT*) output of cylinder position.

The *DMA* controller on the personal computer motherboard is programmed to read 20 single 16 bit words and store them sequentially in a given memory location for each transfer. It is also programmed to reload the initial address for the next transfer after each transfer of 20 readings is complete. When a reading is taken, the result is put into a First-in-First-out (*FIFO*) on the *A/D* board and a *DMA* request is issued. The *DMA* controller on the motherboard retrieves the data and stores it in system ram (in sequence). When the 20th reading is stored, the *DMA* controller asserts a signal that is looped back to an interrupt line by the *A/D* board. At this point, control is given to the Controller *ISR*. The controller sends 5 packets of data: a packet to transmit maximum load reading; a packet to transmit the minimum load reading; a packet to trigger an ultrasonic reading at low load, a packet to trigger video at high load and a packet to trigger ultrasonic readings at high load.

The test apparatus is equipped with four different sensing devices including:

- a) *A travelling optical microscope* for monitoring surface cracks during fatigue damage evolution;
- b) *An Ultrasonic flaw detector* for detection of microstructural damage during early stages of fatigue damage;
- c) *An Extensometer (LVDT)* for position measurements; and

d) A *Load cell* for load measurements.

### 3.1. Geometry of the Test Specimens

The specimens used in the experimental apparatus are typical hourglass shaped flat plates that have a machined notch for a stress riser to guarantee crack propagation at the notch end. Specimens used in this study are made of 7075-T6 aluminium alloy. In this chapter, different specimens with either a center notch or a side notch geometry are used for fatigue experiments. These specimens with local stress concentration regions are designed to break in a reasonably short period of time to enhance the speed of the experiments. The geometries of the two different specimens are presented below:

- *Specimens with center notch geometry*: Figure 2 shows a typical center notched specimen (left image) used for testing in the fatigue damage test apparatus. This specimen has a notch at the center that is made to increase the stress concentration factor to ensure crack initiation and propagation at the notch ends. The specimens of this configuration are 3 mm thick and 50 mm wide, and have a slot of 1.58 mm  $\times$  4.5 mm at the center.
- *Specimens with side notch geometry*: Figure 2 also shows a typical compact specimen (right image) with a notch on one side. The specimens of this configuration are 3 mm thick and 50 mm wide with a slot on one side of 1.58 mm diameter and 4.57 mm length.

The test specimens are subjected to sinusoidal loading under tension-tension mode (i.e., with a constant positive offset) at a frequency of 12.5 Hz. The direct component (*DC*) offset is provided in the load cycling to ensure that the specimen is always under tension. Since inclusions and flaws are randomly distributed across the material small cracks appear at these defects and propagate and join at the machined surface of the notch even before microscopically visual cracks appear on the surface. Table 1 provides the material properties of 7075-T6 aluminium specimens.

### 3.2. Sensors for Damage Detection

The fatigue damage testing apparatus is equipped with a variety of damage sensors [47]. Two types of sensors that have been primarily used for damage detection are: a) *the travelling optical microscope* and b) *the ultrasonic flaw detector*.

#### 3.2.1. Travelling Optical Microscope

The travelling optical microscope, shown as part of the test apparatus in Figure 1, provides direct measurements of the visible part of a crack. The primary instrument for measuring crack length is a Questar QM100 Step Zoom Long distance microscope. This microscope is mounted on a 3-axis stepper motor driven precision stage. The resolution of the optical microscope is about 2 microns at a working distance of 10 to 35 cm.

The microscope can also be focused at different magnifications. The images are taken at a magnification of 75x. The long distance between the microscope and the specimen

**Table 1. Properties of 7075-T6 specimens**

Physical Property	Value
Tensile Strength, Ultimate	570 MPa
Tensile Strength, Yield	505 MPa
Modulus of Elasticity	72 GPa
Fatigue Strength	160 MPa
Poisson's Ratio	0.33
Shear Modulus	26.9 GPa
Shear Strength	330 MPa

is a key feature, because it allows mounting of sensor probes without interference from the microscope optics. The microscope is used as the lens for a digital 8-bit monochrome progressive scan (non-interlaced) video camera that is capable of asynchronous operation (i.e., is not limited to a constant frame rate like a normal video camera).

Since the crack tip moves out of the field of view of the microscope during the test, the motorized stage is used to move the microscope in coordination with the progress of the crack. The growth of surface crack is monitored continuously by the microscope which takes the images of the specimen surface at regular intervals. In order to take pictures, the controller slows down the machine to less than 5 Hz to obtain a better resolution of the images. In the experiments with a center notch geometry, the microscope shifts from left to right side of the central notch and vice versa after every 200 cycles to track crack growth on both sides of the notch. The data acquisition software also allows for manual operation and image capture at the desired moment.

Figure 3 shows typical images of a broken specimen. The semi-circular region visible in Figure 3 is the notch. Two different stages of fatigue crack growth are shown: a) first appearance of a crack on the surface of the specimen and b) almost broken specimen with a very large crack growth. One observation from these figures indicates that the profile of crack growth is not always a straight line. The crack tip tends to propagate in the direction where there is the least resistance to crack growth.

The crack length can be measured by moving the microscope with the help of a user friendly software interface such that a cursor superimposed on the microscope image is over the crack tip. The traveled distance is denoted as the crack length measured from the notch end. The operator records the initial position of the notch edge(s). As the crack propagates, the operator periodically moves the microscope until the cursor is over the crack tip, saves a microscope image, and saves the motion stage position, i.e. crack tip position. The saved images are displayed in a separate window and it is possible to review the images during the test. The position of the crack tip is saved so that the motion controller can be used to quickly return to the crack tip location from anywhere in the range of motion of the stage. The position of all three stages is recorded so that the proper focus and elevation are

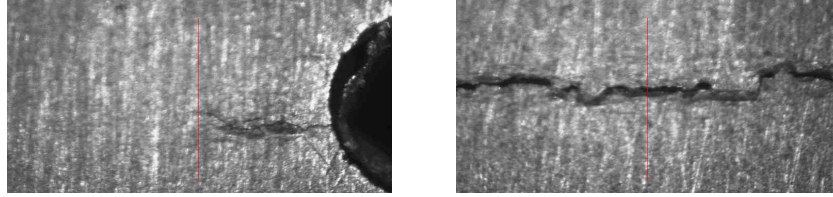


Figure 3. Images of a specimen as captured by the optical microscope indicating the first appearance of a surface crack (left image) and a fully developed large crack (right image).

maintained.

The major weakness of the optical method is that the crack must be visible on the side of the specimen that is being observed, or for convenience, the front. One unfortunate circumstance is that a crack initiates on the back side of the specimen, and propagates through the specimen's entire thickness. Furthermore, the microscope is unsuitable for most field applications.

### 3.2.2. Ultrasonic Flaw Detector

As a ductile alloy structure is commonly subjected to fatigue failure, a large portion of its service life is spent in crack initiation and in the presence of very small cracks. The objective of this research is to acquire knowledge of the damage evolution during the major part of service life at the crack initiation stage, and not simply at the crack propagation stage when the life is largely expended. There are very few methods for detection of microstructural flaws and extremely small cracks in ductile materials. There are fewer still that are suitable for installations outside of the laboratory in actual field operations. Ultrasonic flaw detection meets the requirements of real time damage sensing on structures in service. Ultrasonic flaw detectors are commonly used in the aerospace and nuclear power industries to detect flaws in structures, and have been used by many researchers for crack length measurements in laboratory environment [48].

The ultrasonic flaw detector functions by emitting high frequency ultrasonic pulses that travel through the specimen and return back through the receiver transducers. A piezoelectric transducer is used to inject ultrasonic waves in the specimen and an array of receiver transducers is placed on the other side of notch to measure the transmitted signal, as seen in Figure 4. A Matec TB1000 Gated Amplifier PC add-in card drives a piezoelectric transducer with a sine wave with amplitude of 300V. To be more explicit, the excitation signal consists of short bursts of a sine wave of constant amplitude interrupted by relatively long periods of inactivity at 0V. The wedges, used for the transducers in the tests, have a high enough slope angle that the signal takes multiple paths through the test article and reach the pickup transducers.

In the experiments for central notched specimens, an array of 2 receiver transducers is placed below the notch to detect faults on both left and right side of the notch. In case of the compact specimens, a single receiver transducer is placed under the notch to detect fatigue damage at the notch tip. The ultrasonic waves are generated as 10MHz sine wave signals. The ultrasonic system is synchronized with the load cycling such that the waves are

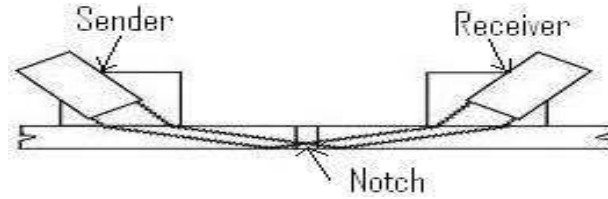


Figure 4. Ultrasonic flaw detection scheme.

emitted during a very short portion at the peak of every load cycle ( $\sim 12.5\text{Hz}$ ). Ultrasonic measurements are taken at stress levels that exceeded the crack opening stress. The crack is open when the specimen is under maximum stress at the peak of a load cycle and this causes maximum attenuation of the ultrasonic waves. Note that if the crack closure occurs at low loads, then an alternative method would be needed to detect anomalies.

The sender and receiver ultrasonic transducers are placed on two positions, above and below the central notch, so as to send the signal through the region of crack propagation and receive it on the other side, as seen in Figure 4. As with the propagation of any wave, it is possible that discontinuities in the propagation media will cause additive and destructive interference. Since material characteristics (e.g., voids, dislocations and short cracks) influence the ultrasonic impedance, a small fault in the specimen is likely to change the signature of the signal at the receiver end. Therefore, the signal can be used to capture some of the minute details and small changes during the early stages of fatigue damage, which may not be possible to detect by an optical microscope [2].

Prior to the appearance of a crack on the surface of the specimen as detected by the optical microscope, deformations (e.g., dislocations and short cracks) inside the specimen cause detectable attenuation and/or distortion of the ultrasonic waves [42]. Recent literature has also shown nonlinear modelling approaches of the ultrasonic wave interference with the material micro-structures [49] [50]. An elaborate description of the properties of ultrasonic waves in solid media is provided by Rose [51].

It is observed that cracks always start at the stress-concentrated region near the notch but the exact site of crack nucleation can be treated as a random event. Formation of very small cracks is difficult to detect and model due to large material irregularities. The ultrasonic technique is easy to install at a potential damage site and is capable of detecting incipient fatigue damage before the onset of widespread fatigue crack propagation. In contrast, an optical microscope is only capable of detecting cracks when they appear on the front surface of the specimen. The ultrasonic instrument is more effective than optical microscopy in measuring the condition of the specimen, since the microscope can only capture the condition on one face of the specimen and the ultrasonic measurements are affected throughout the cross section of the crack. This is particularly the case when the crack is small, because then the 2-D geometry of the crack is not well represented by a measurement on the surface. The study in this chapter is based on analyzing the ultrasonic data for monitoring fatigue damage during both crack initiation and crack propagation stages.

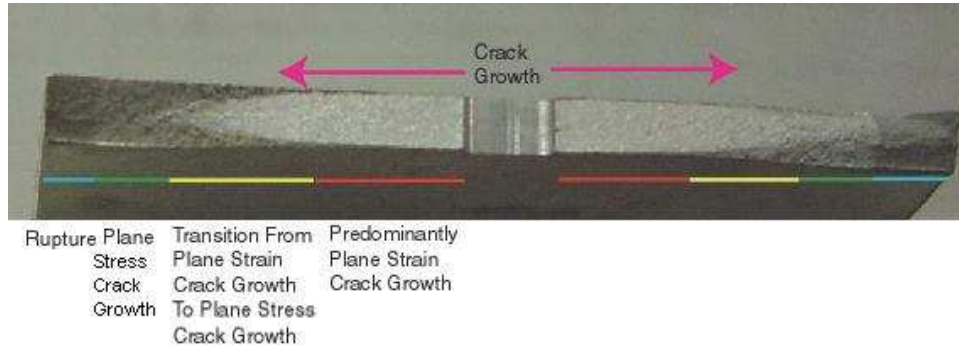


Figure 5. Crack surface showing the macro stages of crack growth [47].

### 3.3. Progression of Fatigue Damage

This section discusses the progression of crack growth as observed in the specimens designed for this study [47]. Although it may seem formulaic for practitioners in fracture mechanics, six stages of crack growth are considered in this research. The first stage is crack initiation. The second stage is two-dimensional (2D) crack growth under plane strain. The third stage is the propagation of a through crack under plane strain. The fourth stage of fatigue growth is a transition from plane strain to plane stress crack growth. The fifth stage of fatigue growth is pure plane stress crack growth. The final stage is rupture, where there is so little residual strength left that the remaining ligament may fail in only a few stress cycles. Figure 5 shows the crack surface of a specimen with different macro stages of crack growth.

The crack initiation stage occurs prior to the formation of a well defined crack and involves mechanisms at a microstructural level. Optical microscopy does not adequately resolve the features of this stage of crack formation, most of which are too small and are not clearly observable on the surface of the specimen. Thus, there is no way to correlate the progression of crack initiation with measurements from other instruments. The other problem is a lack of usable models. Strain-Life is commonly used to model initiation. Strain-life models essentially allocate the observed period of initiation in a fixed pattern. However, initiation is highly uncertain and therefore the models should have a stochastic structure. Thus, however good an analytical model is, it may not be adequate to predict the crack initiation behavior of any given specimen. Since inclusion and flaws are randomly distributed throughout the material, small cracks that form at these defects propagate and join on the machined surface of the notch for a considerable number of cycles before even microscopically small cracks appear on the surface. Figure 6 shows the origin of several small cracks at the edge of the notch as indicated by blue regions. The image is taken by a surface interferometer from ZYGO that provides noncontact three-dimensional quantitative surface topography measurement of the specimen. Using ZYGO's technology of phase-shifting interferometry, the interferometer measures a wide range of surfaces and provides precise 3D profiling and is ideally suited for high resolution measurements on various smooth surfaces.

The 2D stage of crack growth is important for a number of reasons as it is a large source

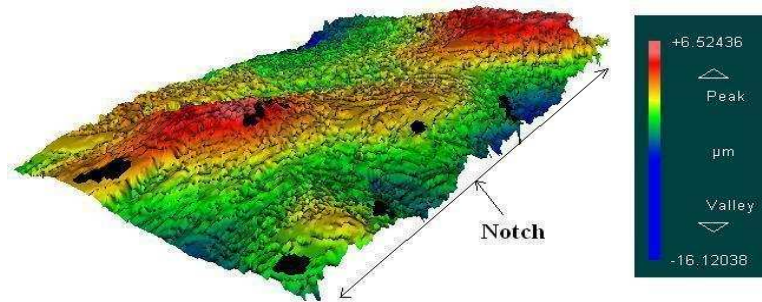


Figure 6. Three dimensional surface profile of a broken specimen. The notch edge is indicated in the figure. The image is taken by a surface interferometer from ZYGO. The colors shown in the legend indicate different depth levels on the surface. As seen in the figure, there are probably three different regions where small cracks developed near the notch.

of variability in the life of a structure. It is possible that 2D cracks have approximately equal length through the thickness and along the width of the specimen. Thus, it might be possible that the 2D stage will last until the surface crack length is equal to the thickness of the specimen. There are three major scenarios for the 2D crack progression on a given side of the notch. The first scenario is that a corner crack forms on both corners of the notch at approximately the same time. These cracks grow independently in roughly semicircular shape until they join in the middle. The relatively small ligament left between the cracks cracks very quickly forming a through crack. This is ideal because the visible portion of the crack on either surface of the specimen is a very good measure of the progress of crack growth for the entire test.

A somewhat less observed scenario is that a penny shaped crack forms in the center of the notch and grow outwards to the edge of the specimen. This phenomenon may result in fairly large crack growth in the center of the specimen before it propagates outward to the surface. However, it is very likely that surface cracks form and join the interior crack before an interior crack propagates to the surface. The most problematic scenario is that a corner crack forms on one surface and propagates through to the other side of the specimen. This results in a crack that is longer on one surface than the other for most part of the test.

In any given test, a mixture of these scenarios will undoubtedly occur. Once one side of the notch has cracked through from one surface to another the third stage of crack growth is started. In center notch specimens, it is extremely unlikely that the crack on one side of the notch will form a through crack at the same time as the other side of the notch. When the cracking of both sides of the notch has formed a through crack, the total crack length has been observed to grow as a center cracked specimen. For a large majority of specimens when the second through crack is formed, it grows much more quickly than the other side. Assuming reasonable stress levels, the bulk of the specimen is in a state of plane strain through the stage where a through center-crack has formed for a considerable portion of the propagation afterwards.

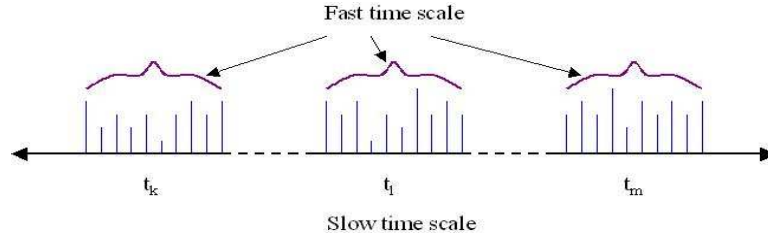


Figure 7. Pictorial view of the two time scales: 1) *slow time scale* where anomalies evolve and 2) *fast time scale* where data acquisition is done.

The material at the surfaces of the specimen is always in plane stress since it is not constrained in the through-thickness direction. For this stage of crack growth, any plasticity in the bulk of the material is constant through the thickness of the specimen as the material is constrained by the material around it. As the localized stress becomes high enough, the stress state of the specimen undergoes a transition from plane strain to plane stress. This is evidenced by the formation of angled area on the surface of the specimen. As this stage progresses, the angled areas grow larger, and the area in the center of the specimen that is still in plane strain gets smaller and eventually disappears. This transition is observable on the surface, since the crack grows in a reasonable facsimile to a straight line when it is in plane strain.

Observing the specimen after it has failed all the way through, it can be seen that the plane strain area in the center of the transition from plane strain to plane stress remains in plane with the crack that formed fully in plane strain. Thus, when the transition from plane strain to plane stress occurs, the crack on the surface starts to move up or down on the surface of the specimen. The final stage of crack growth is rupture, which is a failure of the remaining ligaments in a few cycles.

## 4. Problem Formulation

This section presents the problem formulation for pattern recognition and anomaly detection based on symbolic dynamic filtering (*SDF*) in complex dynamical systems. The underlying concepts and essential features of *SDF* [21][17] are presented in the appendix.

### 4.1. Concept of Two Time Scales for Damage Monitoring

Fatigue damage detection is formulated as a two-time-scale problem as explained below.

- The *fast time scale* is related to the response time of process dynamics. Over the span of a given time series data sequence, the behavioral statistics of the system are assumed to remain invariant, i.e., the process is assumed to have statistically stationary dynamics at the fast time scale. In other words, statistical variations in the internal dynamics of the system are assumed to be negligible on the fast time scale.

- The *slow time scale* is related to the time span over which the process may exhibit non-stationary dynamics due to (possible) evolution of anomalies. Thus, an observable non-stationary behavior can be associated with anomalies evolving at a slow time scale.

A pictorial view of the two time scales is presented in Figure 7. In general, a long time span in the fast time scale is a tiny (i.e., several orders of magnitude smaller) interval in the slow time scale. For example, fatigue damage evolves on a slow time scale, possibly in the order of months or years, in machinery structures that are operated in the fast time scale approximately in the order of seconds or minutes. Hence, the behavior pattern of fatigue damage is essentially invariant on the fast time scale. Nevertheless, the notion of fast and slow time scales is dependent on the specific application, loading conditions and operating environment. As such, from the perspective of fatigue damage monitoring, the sensor data acquisition is done on the fast time scale at different slow time epochs separated by uniform or non-uniform intervals on the slow time scale.

## 4.2. Methodology

The problem of fatigue damage monitoring is formulated to achieve the following objectives:

- *Information-based identification of damage progression patterns* - The possible sources of information can include time series data of appropriate sensors (e.g., ultrasonic) mounted on critical components of the system;
- *Real-time execution* - The analytical tools must be computationally efficient and have the capability of real-time execution on commercially available inexpensive platforms;
- *Capability of small change detection* - The pattern recognition methodology for anomaly detection must be sensitive to small changes and have the capability of providing early warnings of incipient faults. The methodology must also be capable of estimating fault precursors to formulate a decision and control policy for damage mitigation and life extension;
- *Robustness to measurement noise and disturbances* - The pattern recognition tool must be robust to noise and disturbances and must have low probability of false alarms.

Once the appropriate sensor selection is done, the next task is development of analytical tools for analysis of time series data [14]. Various signal processing applications deal with data analysis and attempts have been made to extract maximum useful information from the ensemble of sensor data. The problem of feature extraction from time series data for damage monitoring has been recently addressed by many researchers [52] [53] [54]. The tools of statistical pattern recognition, auto-regressive model analysis, and wavelet analysis were applied to classify faults by different data patterns. However, the critical issue of early detection of gradually evolving faults in a real time setting were not addressed. Moreover,

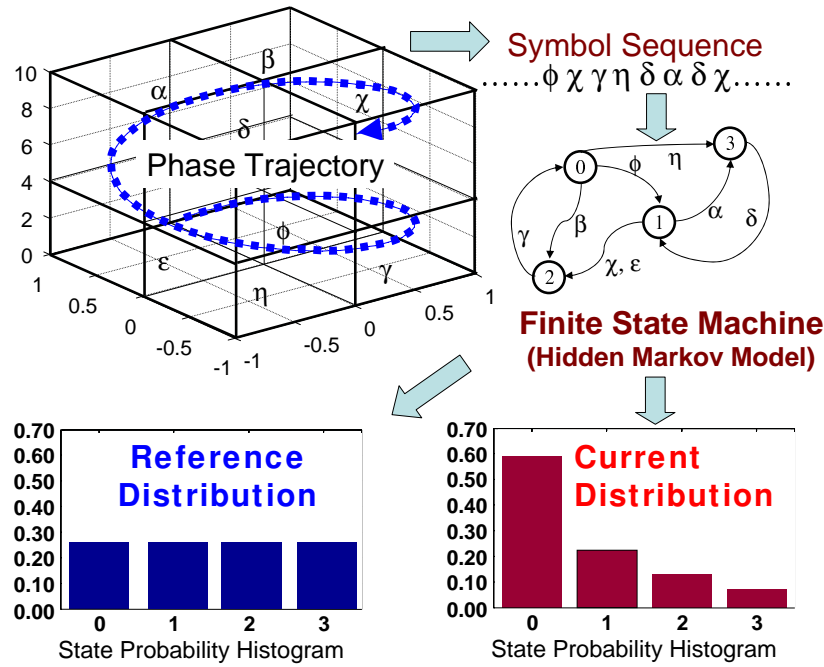


Figure 8. Conceptual view of symbolic dynamic filtering.

no quantifying measure was provided for damage accumulation and growth rate based on statistical information.

Recently, some techniques of nonlinear dynamics have also been applied for damage monitoring [55] [56] [57], which are primarily based on the concepts of attractor-based cross-prediction error between the measured signal and its predicted value. However, since the dimensions of the phase space may grow unbounded for noisy data, this analysis could be computationally expensive and infeasible for real-time applications. Furthermore, dealing with high dimensions might lead to spurious results and dimension reduction may lead to loss of vital information. To alleviate these difficulties, this chapter has adopted a novel method of wavelet-based partitioning [21] [58]. Based on this partitioning, the pertinent information is extracted from time series data sets in the form of probability distributions. Slight deviations in these distributions from that under the nominal condition is captured to identify the damage pattern. This chapter presents symbolic dynamic filtering (*SDF*) [21][17][22][23] to analyze time series data of sensors (e.g., ultrasonic) for detection of precursors leading to crack initiation and eventual widespread fatigue.

The core concept of *SDF* is based on appropriate phase-space partitioning of the dynamical system to yield an alphabet to obtain symbol sequences from time series data [59]. The time series data of appropriate sensors (e.g., ultrasonic) are processed and subsequently converted from the domain of real numbers into the domain of (discrete) symbols [15][18][17]. The resulting symbol sequence is a transform of the original time series sequence such that the loss of information is minimized in the sense of *maximized entropy*. The chapter has adopted wavelet-based partitioning approach for symbol sequence gener-

ation [21] [58]. Wavelet based partitioning approach is robust and is particularly effective with noisy data [58].

Subsequently, tools of Computational Mechanics [21][17][60][61] are used to identify statistical patterns in these symbolic sequences through construction of a (probabilistic) finite-state machine [21][16]. Transition probability matrices of the finite state machines, obtained from the symbol sequences, capture the pattern of the system behavior by means of information compression. For anomaly detection, it suffices that a detectable change in the pattern represents a deviation of the nominal pattern from an anomalous one. The state probability vectors, which are derived from the respective state transition matrices under the nominal and an anomalous condition, yield a statistical pattern of the anomaly. The concept of *SDF* is illustrated in Figure 8.

Symbolic dynamic filtering (*SDF*) for anomaly detection is an information-theoretic pattern recognition tool that is built upon a fixed-structure, fixed-order Markov chain, called the *D-Markov machine* [21][17]. Recent literature [44] [62] has reported experimental validation of *SDF*-based pattern recognition by comparison with other existing techniques such as Principal Component Analysis (*PCA*) and Artificial Neural Networks (*ANN*); *SDF* has been shown to yield superior performance in terms of early detection of anomalies, robustness to noise [58], and real-time execution in different applications such as electronic circuits [62], mechanical vibration systems [63], and fatigue damage in polycrystalline alloys [44].

### 4.3. Procedure for Anomaly Detection

The *SDF*-based anomaly detection requires the following steps:

- *Time series data acquisition on the fast time scale from appropriate sensors* - Collection of data sets is done at different slow time epochs. As stated in the previous subsection, the choice of time scales is dependent on the application and requires an approximate *a priori* knowledge about the time period of evolution of anomalies (e.g., fatigue crack growth).
- *Transformation of time series data from the continuous domain to the symbolic domain* - This is done by partitioning the data (e.g., ultrasonic) into finitely many discrete regions to generate symbol sequences at different slow time epochs [15][18]. The chapter has presented a wavelet-based partitioning scheme for symbol sequence generation.
- *Construction of a finite state machine* - The machine is constructed from the symbol sequence generated at the nominal condition
- *Calculation of the pattern vectors at different slow time epochs* - The elements of these pattern vectors consist of the visiting frequencies of the finite state machine states
- *Identification of behavioral changes*- Fatigue damage detection is based on the information derived from the evolution of the pattern vector at different slow time epochs with respect to the one at the nominal condition

## 5. Forward and Inverse Problems

Fatigue damage monitoring is formulated as a solution of two interrelated problems [21]: (i) *forward problem of Pattern Recognition* for (offline) characterization of the anomalous behavior, relative to the nominal behavior and (ii) *inverse problem of Pattern identification* for (online) estimation of parametric or non-parametric changes based on the knowledge assimilated in the forward problem and the observed time series data of quasi-stationary process response.

The forward problem consists of prediction of outcomes, given a priori knowledge of the underlying model parameters. In absence of an existing model this problem requires generation of behavioral patterns of the system evolution through off-line analysis of an ensemble of the observed time series data. The objective of the inverse problem is to infer the anomalies and to provide the estimates of the remaining useful life from the observed time series data in real time based on the information generated during the forward problem. Inverse problems arise in different engineering disciplines such as geophysics, structural health monitoring, weather forecasting, and astronomy. Inverse problems often become ill-posed and challenging due to the following reasons: (a) high dimensionality of the parameter space under investigation and (b) in absence of a unique solution where change in multiple parameters can lead to the same observations. That is, it may not always be possible to identify a unique anomaly pattern based on the observed behavior of the dynamical system. Nevertheless, the feasible range of parameter variation estimates can be narrowed down from the intersection of the information generated from inverse images of the responses under several stimuli.

In presence of sources of uncertainties, any parameter inference strategy requires estimation of parameter values and also the associated confidence intervals, or the error bounds, to the estimated values. As such, inverse problems are usually solved using the Bayesian methods that allow observation based inference of parameters and provide a probabilistic description of the uncertainty of inferred quantities. A good discussion of inverse problems is presented by Tarantola [64].

The algorithms of *SDF* can be implemented to solve both these problems. In context of fatigue damage monitoring, the tasks and solution steps of these two problems as followed in this chapter are discussed below.

### 5.1. Forward Problem

The primary objective of the forward problem is identification of changes in the behavioral patterns of system dynamics due to evolving anomalies on the slow time scale. Specifically, the forward problem aims at detecting the deviations in the statistical patterns in the time series data, generated at different time epochs in the slow time scale, from the nominal behavior pattern. The solution procedure of the forward problem requires the following steps:

- F1. Collection of time series data sets (at fast time scale) from the available sensor(s) at different slow time epochs;
- F2. Analysis of these data sets using the *SDF* method as discussed in earlier sections to generate pattern vectors defined by the probability distributions at the corresponding

slow time epochs. The profile of anomaly measure (see Appendix A.1.) is then obtained from the evolution of this pattern vector from the nominal condition;

- F3. Generation of a family of such profiles from multiple experiments performed under identical conditions to construct a statistical pattern of damage growth. Such a family represents the uncertainty in the evolution of fatigue damage due to its stochastic nature. The uncertainty arises from the random distribution of microstructural flaws in the body of the component leading to a stochastic behavior [11].

## 5.2. Inverse Problem

The objective of the inverse problem is to infer the anomalies and to provide estimates of system parameters from the observed time series data and system response in real time. The decisions are based on the information derived in the forward problem. For eg., in the context of fatigue damage, identical structures operated under identical loading and environmental conditions show different trends in the evolution of fatigue due to surface and sub-surface material uncertainties. Therefore, as a precursor to the solution of the inverse problem, generation of an ensemble of data sets is required during the forward problem for multiple fatigue tests conducted under identical operating conditions. Damage estimates can be obtained at any particular instant in a real-time experiment with certain confidence intervals using the information derived from the ensemble of data sets of damage evolution generated in the forward problem [21]. The solution procedure of the inverse problem requires the following steps:

- I1. Collection of time series data sets (in the fast time scale) from the available sensor(s) at different slow time epochs up till the current time epoch in a real-time experiment as in step F1 of the forward problem;
- I2. Analysis of these data sets using the *SDF* method to generate pattern vectors defined by probability distributions at the corresponding slow time epochs. The value of anomaly measure at the current time epoch is then calculated from the evolution of this pattern vector from the nominal condition (see Appendix A.1.). The procedure is similar to the step F2 of the forward problem. As such, the information available at any particular instant in a real-time experiment is the value of the anomaly measure calculated at that particular instant;
- I3. Detection, identification and estimation of an anomaly (if any) based on the computed anomaly measure and the statistical information derived in step F3 of the forward problem.

A schematic of the overall framework for the fatigue damage monitoring problem in mechanical systems is shown in Figure 9. As shown in Figure 9, the forward problem section involves the generation of ultrasonic data sets from fatigue experiments which are analyzed using the *SDF* method to produce a profile of the anomaly measure (see Appendix) that represents the evolution of fatigue damage. Following the same procedure, several experiments are conducted under identical conditions to generate a family of anomaly measure

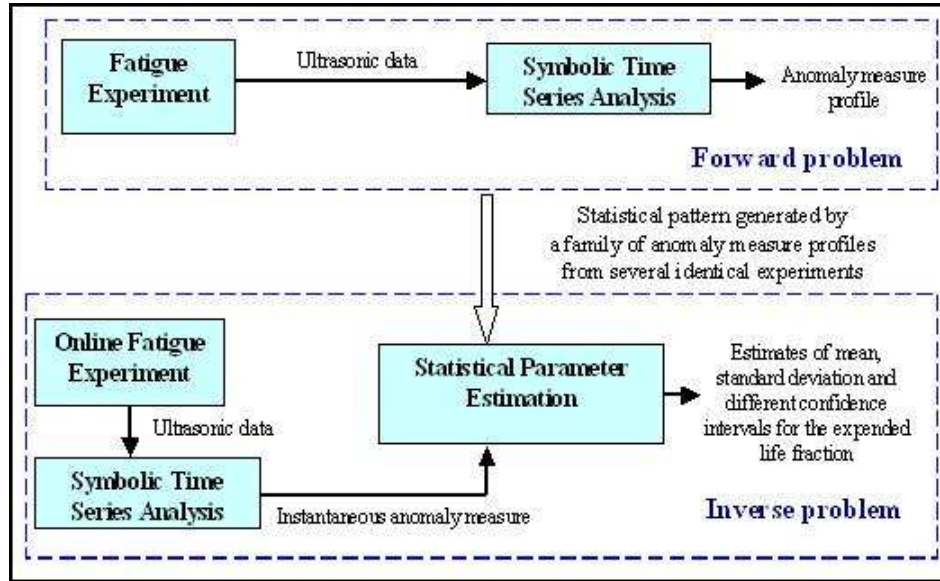


Figure 9. Framework of *SDF* based fatigue damage detection in mechanical systems.

profiles. Such a family represents the stochastic behavior of the fatigue damage evolution on a slow time scale (see Section 7.1.).

This family of anomaly measure profiles is analyzed in the inverse problem section to generate the requisite statistical information (see Section 7.2.). The information available in real time is the value of the anomaly measure obtained from the analysis of ultrasonic data at any particular time epoch. This information is entered in the inverse problem section that provides the estimates of the *expended life fraction*. The estimates can only be obtained within certain bounds at a particular confidence level. The online statistical information of the damage status is significant because it can facilitate early scheduling for the maintenance or repair of critical components or to prepare an advance itinerary of the damaged parts. The information can also be used to design control policies for damage mitigation and life extension.

## 6. Real-time Fatigue Damage Detection

The fatigue tests were conducted using center notched specimens, made of the Aluminum alloy 7075-T6, at a constant amplitude sinusoidal load for a low-cycle fatigue, where the maximum and minimum loads were kept constant at 87MPa and 4.85MPa. A significant amount of internal damage occurs before the crack appears on the surface of the specimen when it is observed by the microscope [65]. However, it is also possible that the crack appears on the other surface of specimen or on the surface of the notch.

This surface or sub-surface damage caused by multiple small cracks and microstructural damage affects the ultrasonic waves when they pass through the region where these faults have developed. This phenomenon causes signal distortion and attenuation at the receiver end. The crack propagation stage starts when this internal damage eventually develops into

a single large crack. Subsequently, the crack growth rate increases rapidly and when the crack is sufficiently large, complete attenuation of the transmitted ultrasonic signal occurs, as seen at the receiver end. This sudden sharp change in the rate of progression of fatigue damage is clearly visible after the crack appears on the surface. The rapid change in the statistical patterns of the ultrasonic data also indicate the onset of crack propagation. After the crack appears on the surface, fatigue damage growth can be easily monitored by the microscope but the ultrasonics provide early warnings even during the crack initiation phase.

### 6.1. Experimental Procedure

The ultrasonic sensing device is triggered at a frequency of 5 MHz at each peak of the ( $\sim 12.5$  Hz) sinusoidal load. The slow time epochs were chosen to be 3000 load cycles (i.e.,  $\sim 240$  sec) apart. At the onset of each slow time epoch, the ultrasonic data points were collected on the fast time scale of  $\sim 8$  sec, which produced a string of 10,000 data points. It is assumed that during this fast time scale, no major changes occurred in the fatigue crack behavior. The nominal condition at the slow time epoch  $t_0$  was chosen to be 5.0 kilocycles to ensure that the electro-hydraulic system of the test apparatus had come to a steady state and that no significant damage occurred till that point. The anomalies at subsequent slow-time epochs,  $t_1, t_2, \dots, t_k, \dots$ , were then calculated with respect to the nominal condition at  $t_0$ .

### 6.2. Data Analysis using Symbolic Dynamic Filtering (*SDF*)

Following the *SDF* procedure for anomaly detection, the alphabet size for partitioning was chosen to be  $|\Sigma| = 8$  and window length of  $D = 1$ , while the mother wavelet chosen to be ‘gaus2’ [66]. (Absolute values of the wavelet scale series data were used to generate the partition because of the symmetry of the data sets about their mean.) The wavelet basis, ‘gaus2’, provides better results than the wavelet bases of the Daubechies family [67] because the ‘gaus2’ wavelet base closely matches the shape of the ultrasonic signals [58]. This combination of parameters was capable of capturing the anomalies earlier than the optical microscope. Increasing the value of  $|\Sigma|$  further did not improve the results and increasing the value of  $D$  created a large number of states of the finite state machine, many of them having very small or zero probabilities, and required larger number of data points at each time epoch to stabilize the state probability vectors. State probability vector  $\mathbf{p}^0$  was obtained at the nominal condition of time epoch  $t_0$  and the state probability vectors  $\mathbf{p}^1, \mathbf{p}^2, \dots, \mathbf{p}^k, \dots$  were obtained at other slow-time epochs  $t_1, t_2, \dots, t_k, \dots$ . It is emphasized that the anomaly measure is relative to the nominal condition which is fixed in advance and should not be confused with the actual damage at an absolute level.

### 6.3. Results and Discussion

The six triplets of plates in Figure 10 show two-dimensional images of a specimen surface, ultrasonic data and histograms of probability distribution of automaton states at six different time epochs, approximately 5, 30, 40, 45, 60 and 78 kilocycles, exhibiting gradual evolution of fatigue damage [68]. In each triplet of plates from (a) to (f) in Figure 10, the

top plate exhibits the surface image of the test specimen as seen by the optical microscope. As exhibited on the top plates, the crack originated and developed on the right side of the notch at the center. Histograms in the bottom plates of six plate triplets in Figure 10 show the evolution of the state probability vector corresponding to fatigue damage growth on the test specimen at different slow time epochs, signifying how the probability distribution gradually changes from uniform distribution (i.e., minimal information) to delta distribution (i.e., maximum information). The middle plates show the ultrasonic time series data collected at corresponding slow time epochs. As seen in Figure 10, the visual inspection of the ultrasonic data does not reveal much information during early stages of fatigue damage but the statistical changes are captured in the corresponding histograms.

The top plate in plate triplet (a) of Figure 10 shows the image at the nominal condition ( $\sim 5$  kilocycles) when the anomaly measure is taken to be zero, which is considered as the reference point with the available information on potential damage being minimal. This is reflected in the uniform distribution (i.e., maximum entropy) as seen from the histogram at the bottom plate of plate pair (a). Both the top plates in plate triplets (b) and (c) at  $\sim 30$  and  $\sim 40$  kilocycles, respectively, do not yet have any indication of surface crack although the corresponding bottom plates do exhibit deviations from the uniform probability distribution. This is an evidence that the analytical measurements, based on ultrasonic sensor data, produce damage information during crack initiation, which is not available from the corresponding optical images.

The top plate in plate triplet (d) of Figure 10 at  $\sim 45$  kilocycles exhibits the first noticeable appearance of a  $\sim 300$  micron crack on the specimen surface, which may be considered as the boundary of the crack initiation and propagation phases. This small surface crack indicates that a significant portion of the crack or multiple small cracks might have already developed underneath the surface before they started spreading on the surface. The histogram of probability distribution in the corresponding bottom plate shows further deviation from the uniform distribution at  $\sim 5$  kilocycles. The top plate in plate triplet (e) of Figure 10 at  $\sim 60$  kilocycles exhibits a fully developed crack in its propagation phase. The corresponding bottom plate shows the histogram of the probability distribution that is significantly different from those in earlier cycles in plate triplets (a) to (d), indicating further gain in the information on crack damage. In this case, the middle plate also shows significant drop in the amplitude of ultrasonic signals due to development of a large crack. The top plate in plate triplet (f) of Figure 10 at  $\sim 78$  kilocycles exhibits the image of a completely broken specimen. The corresponding bottom plate shows delta distribution indicating complete information on crack damage. The middle plate shows a complete attenuation of the ultrasonic signals.

The normalized anomaly measure curve in Figure 11 shows a possible bifurcation where the slope of the anomaly measure changes dramatically indicating the onset of crack propagation phase. First appearance of a fatigue crack on the surface of the specimen was detected by the optical microscope at approximately 45 kilocycles, which is marked by the dashed vertical line in Figure 11. The slope of the anomaly measure represents the anomaly growth rate while the magnitude indicates the changes that have occurred relative to the nominal condition. An abrupt change in the slope (i.e., a sharp change in the curvature) of anomaly measure profile provides a clear insight into a forthcoming failure. The critical information lies in the region to the left of the vertical line where no crack was visible on the

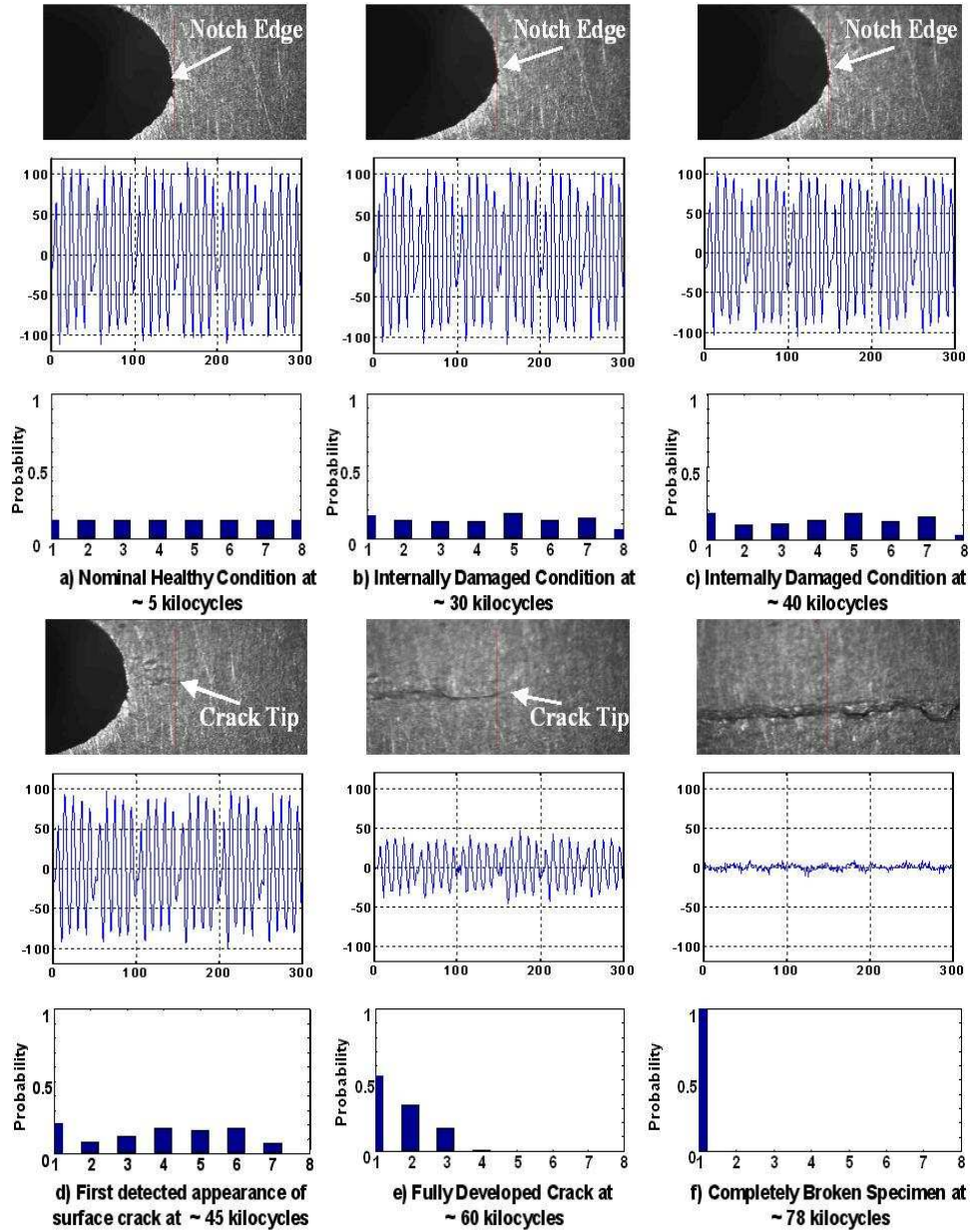


Figure 10. Pictorial view of the evolving fatigue crack damage, corresponding ultrasonic data and histograms of probability distribution [68].

surface. The slope of anomaly measure curve showed a clear trend of growth of anomaly right after ~15 kilocycles. This was the region where multiple small cracks were possibly formed inside the specimen, which caused small changes in the ultrasonic signal profile. Fatigue damage detection using *SDF* of ultrasonic data has been successfully implemented in real time [44].

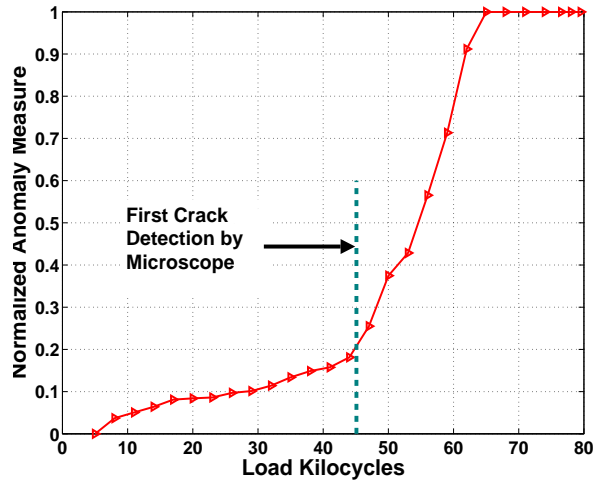


Figure 11. Fatigue damage detection.

#### 6.4. Real-time Implementation

Fatigue damage detection via symbolic dynamic filtering (*SDF*) has been successfully implemented in real time. The nominal condition is chosen after the start of the experiment at time epoch  $t_0$ , when the system attains a steady state and is considered to be in the healthy condition with zero anomaly measure. The function module for *SDF* is triggered at this point. The *D*-Markov machine states are fixed in advance using *a priori* determined values of the parameters: alphabet size  $|\Sigma|$  and window length  $D$ . The tasks of wavelet space partitioning and *D*-Markov machine construction are performed based on the time series data at the slow-time epoch  $t_0$  (nominal condition).

The state probability vector  $\mathbf{p}^0$  at time epoch  $t_0$  is stored for computation of anomaly measures at subsequent slow time epochs,  $t_1, t_2, \dots, t_k, \dots$ , which are chosen to be separated by uniform intervals of time in these experiments. The ultrasonic data acquisition software has a subroutine that writes the time series data of ultrasonic signals into text files at time epochs  $t_0, t_1, \dots, t_k, \dots$ . These text files are then transferred to the function module for anomaly detection such that the *STSA*-based algorithm can read the data from the text files to calculate the anomaly measure at the specified time epochs. The algorithm is computationally very fast (i.e., several orders of magnitude faster relative to slow-time-scale damage monitoring) and the results can be easily plotted on the screen such that the evolution of anomaly measure is exhibited in real time. The plot is updated with the most recent value of anomaly measure at each (slow-time) epoch. Thus, the *SDF* algorithm allows on-line health monitoring and is capable of issuing warnings of incipient failures well in advance.

### 7. Real-time Estimation of Remaining Useful Life

The analytical tool for fatigue damage estimation is based on an ensemble of stochastic data of ultrasonic signals that is generated from a set of identical experiments [46]. The

stochastic data represents the behavioral pattern of fatigue damage evolution. A statistical analysis procedure of this stochastic data is developed to obtain the estimates of the fraction of used fatigue life that in turn can provide the estimate of the remaining useful life in real time. A set of experiments have been conducted and the results are provided for application and validation of the proposed statistical approach.

As discussed in Section 5., the fatigue damage monitoring problem including damage detection and estimation of remaining useful life, is partitioned into two sub-problems: 1) the *forward (or analysis) problem* and 2) the *inverse (or synthesis) problem*. The previous section presented the results of real-time fatigue damage detection that only requires detection of any deviation in the statistical patterns of ultrasonic data from the nominal condition. However, for real-time estimation of the remaining useful life a complete solution of both the forward and the inverse problems is required. This section presents the results of real-time fatigue life estimation.

## 7.1. Solution of the Forward Problem

This subsection presents a detailed description of the solution procedure of the forward problem. As discussed earlier, the primary objective of the forward problem is to identify the behavioral pattern of damage evolution in a complex dynamical system involving the uncertainties (if any) which can be both parametric or non-parametric in nature.

### 7.1.1. Sources of Uncertainties

In case of fatigue damage, the sources of uncertainties include:

- a) material inhomogeneities such as voids or inclusions,
- b) surface defects including finishing marks that usually develop from the machining process, nonuniform polishing and other deformities,
- c) sub-surface defects originating due to random distribution of microstructural flaws like dislocations and grain boundaries,
- d) Variations in the critical dimensions of the components resulting from the non-zero tolerances of the cutting tools used in the fabrication process,
- e) small fluctuations in the environmental conditions such as humidity and temperature,
- f) small fluctuations in the operating conditions due to noisy environment and finite precision of the mechanical system.

In the presence of above uncertainties, a complete solution of anomaly detection problem cannot be obtained in the deterministic setting because the profile of anomaly progression would not be identical for similarly manufactured components. In that case, the problem can be represented in the stochastic setting, where a family of anomaly progression profiles are generated from multiple experiments conducted under identical conditions [69]. As such, the requirement of the forward problem is to generate a pattern that consists of a family of anomaly progression profiles. Each member of this family represents the anomaly

measure profile of a particular sample. This profile is generated from a fatigue test that is conducted to observe the entire service life of the specimen from the healthy condition to the eventual failure.

### 7.1.2. Experimental Procedure

The fatigue tests were conducted on 7075-T6 aluminum specimens at 12.5 Hz frequency. In this case the compact specimens were used. The specimen were subjected to a sinusoidal load cycling where the maximum and minimum loads are 89.3MPa and 4.85MPa at the nominal condition. Ultrasonic waves with a frequency of 10 MHz are triggered at the peak of each sinusoidal load cycle where the stress is maximum and the crack is open causing maximum attenuation of the ultrasonic waves. Since the ultrasonic frequency is much higher than the load cycling frequency, data collection is performed for a very short interval in the time scale of load cycling. The slow time epochs have been chosen to be 1000 load cycles (i.e.,  $\sim 80$  sec) apart. At the onset of each slow time epoch, the ultrasonic data points are collected on the fast time scale of 50 cycles (i.e.,  $\sim 4$  sec), which produced a string of  $N = 15,000$  data points. It is assumed that during the fast time scale of 50 cycles, the system remains in a stationary condition and no major changes occur in the fatigue damage behavior. These sets of time series data points collected at different slow time epochs are analyzed using the *SDF* method (see Appendix) to calculate the anomaly measures at those slow time epochs.

### 7.1.3. Data Analysis using Symbolic Dynamic Filtering (*SDF*)

The nominal condition at the slow time epoch  $t_0$  is chosen to be  $\sim 0.5$  kilocycles to ensure that the electro-hydraulic system of the test apparatus had come to a steady state and it is assumed that no significant damage occurred till that point. This nominal condition is chosen as a benchmark where the anomaly measure is chosen to be zero. The anomalies at subsequent slow time epochs,  $t_1, t_2, \dots, t_k \dots$ , are then calculated using *SDF* to yield a profile of anomaly measure representing the progression of fatigue damage on the slow time scale. The data collection is stopped at a time epoch  $t_f$  considered as the final failure point where the ultrasonic energy is attenuated to 2% of the nominal condition. The energy of the signal is defined as:

$$E = \sum_{i=1}^N |s(i)|^2$$

where  $|s(i)|$  is the magnitude of the  $i^{th}$  data point of the ultrasonic signal. Once the failure point is reached the specimen is already under crack propagation stage and a sufficiently large crack has developed such that it is no longer useful and is considered as broken. Following the above procedure, a family of profiles is generated for multiple experiments conducted under identical experimental conditions.

For the *SDF* procedure, the alphabet size for partitioning has been chosen to be  $|\Sigma| = 8$  and window length of  $D = 1$ , while the wavelet basis is chosen to be 'gaus2' [66]. The algorithm is readily implemented in real-time and is computationally very fast in the sense

that the code execution time is several orders of magnitude smaller than the interval between two adjacent slow time epochs.

#### 7.1.4. Generation of Statistical Patterns

Similar to the procedure described above, ultrasonic time series data are generated under both nominal and anomalous conditions at different slow time epochs for multiple experiments conducted on identically manufactured specimens under identical experimental conditions. *SDF* based analysis of the data from each of these experiments produce a profile of anomaly measure thereby generating an ensemble of anomaly measure profiles for multiple experiments. This family of profiles represents a stochastic pattern of the progression of fatigue damage under identical experimental conditions. To this effect,  $\ell = 40$  experiments have been conducted and the profiles of anomaly measures are shown in Figure 12. The family of the anomaly measure profiles of these experiments is plotted versus a normalized variable, *expended life fraction*,  $\tau_e = \left( \frac{t-t_0}{t_f-t_0} \right)$ , where  $t$  is the actual number of cycles,  $t_0$  is the nominal condition chosen to be  $\sim 0.5$  kilocycles for each experiment and  $t_f$  is the final time of failure for each experiment as described in the previous section. [Note: The *expended life fraction*  $\tau_e$  is normalized between 0 and 1.]

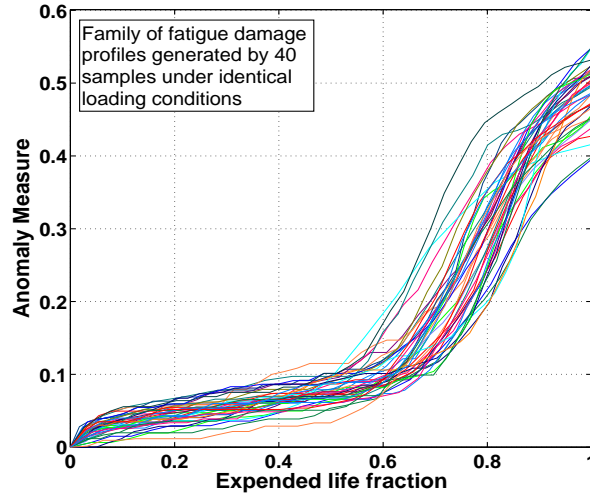


Figure 12. Statistical behavior of fatigue damage represented by a family of anomaly measure profiles generated by 40 identical experiments [46].

For each individual experiment, the state probability vector  $\mathbf{p}^0$  is generated at the nominal condition  $t_0$  by partitioning the wavelet domain using the maximum entropy principle [58]. As a consequence,  $\mathbf{p}^0$  has uniform distribution, i.e. each element has equal probability. In contrast, for the completely broken stage of the specimen, the entire probability distribution is concentrated in only one element of the state probability vector, i.e. delta distribution, which indicates a very large attenuation of the ultrasonic signal [44]. Therefore, as the fatigue crack damage evolves, the uniform distribution (i.e., maximum entropy)

under nominal condition degenerates toward the delta distribution (i.e., zero entropy) for the broken specimen. Since,  $\mathbf{p}^0$  has uniform distribution for all experiments, the statistical property is identical for all experiments at the nominal condition.

As seen in Figure 12, each profile has a smaller slope of the anomaly measure during the initial period of fatigue damage, i.e., the crack initiation region. Anomaly measure gradually increases during this period where small microstructural damage occurs in the specimen. During the end stage of this period small micro cracks eventually develop into a single large crack leading to a transition from the crack initiation stage to the crack propagation stage (approx from  $\tau_e = 0.5$  to  $\tau_e = 0.7$ ). This phenomenon is observed by a sharp change in the slope of the anomaly measure profile of each sample. Once the crack propagation stage starts the fatigue damage occurs rapidly eventually leading to the final failure.

## 7.2. Solution of the Inverse Problem

The objective of the inverse problem is identification of anomalies and estimation of the fault parameters based on the family of curves generated in the forward problem [46]. It is essential to detect the evolving fatigue damage and to estimate the remaining useful life during the operating period of the mechanical system, so that appropriate remedial action(s) can be taken before the onset of widespread fatigue propagation leading to complete failure. Therefore, estimation of fatigue damage is crucial for scheduled maintenance.

### 7.2.1. Generation of the Pattern Matrix

In an online experiment, time series data sets (at fast time scale) of the ultrasonic sensors are generated at different slow time epochs up till the current time epoch. These data sets are analyzed using *SDF* method as discussed in Appendix Appendix A. to generate the probability distributions at the corresponding slow time epochs. The value of anomaly measure at the current time epoch is then calculated from the evolution of this probability vector from the nominal healthy condition. As such, the information available at any particular instant in a real time experiment is the value of anomaly measure calculated at that particular instant. Based on this derived value of the anomaly measure the exact determination of the *expended life fraction* ( $\tau_e$ ) is not possible due to the variations observed in the statistical family as seen in Figure 12. Therefore, due to uncertainty in determining its exact value at a particular value of anomaly measure,  $\tau_e$  can be treated as a random variable [65].

The range of anomaly measure (i.e. the ordinate in Figure 12) is partitioned into  $h = 100$  uniformly spaced levels. A pattern matrix  $\mathcal{T}$  of dimension  $\ell \times h$  is then derived from the anomaly measure profiles shown in Figure 12. The elements of  $\mathcal{T}$  are derived such that each column of  $\mathcal{T}$  corresponds to the values of  $\tau_e$  measured for  $\ell$  samples at the corresponding anomaly measure. As such, the elements of each column of  $\mathcal{T}$  describe a distribution of the random variable  $\tau_e$ .

### 7.2.2. Estimation of the Expended Life Fraction

In order to estimate the value of  $\tau_e$  by statistical means, a two-parameter *lognormal* distribution [13] [70] is hypothesized for each column of  $\mathcal{T}$ . Lognormal distribution is obtained

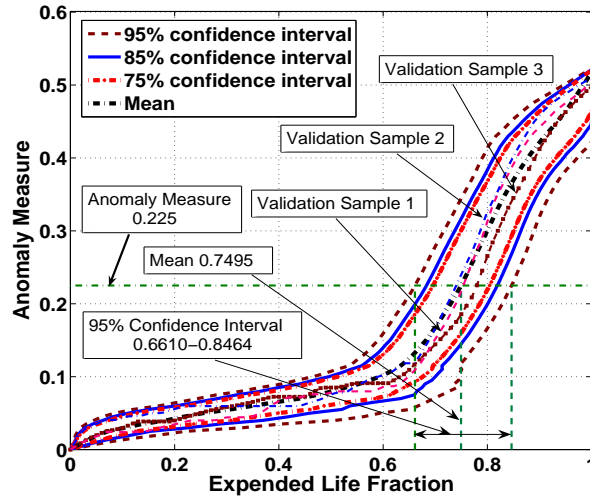


Figure 13. Plots of confidence interval bounds are shown at three different confidence levels of 95%, 85% and 75%. Profiles of anomaly measure are also shown for three new validation test specimens [46].

for each column of  $\mathcal{T}$  over the mean and the variance of  $\tau_e$ . The goodness of fit is examined by both  $\chi^2$  and Kolmogorov–Smirnov tests [71]. The number of bins were taken to be  $r = 8$  for the data set of each column of  $\mathcal{T}$ . With  $f = r - 2 - 1 = 5$  degrees of freedom, the  $\chi^2$ -test shows that, for each of the  $h$  data sets, the hypothesis of the two-parameter log-normal distribution passed the 20% significance level [71] which suffices the conventional standard of 5% significance level. Also, for each of the  $h$  data sets, the hypothesis passed the 20% significance level of the Kolmogorov–Smirnov test which again suffices the conventional standard of 5% significance level. A good discussion of these statistical tests is provided in reference [71].

Once the lognormal distributions are obtained, the confidence intervals bounds at different confidence levels can be computed from the properties of the distribution using elementary statistics [71] [72]. Confidence level signifies the probability that the estimated parameter will lie within the corresponding confidence interval. As an example, for a confidence level of 95%, the probability that the actual parameter will lie between the specified confidence interval is 95%. Figure 13 provides the plots of confidence interval bounds at three different confidence levels of 95%, 85% and 75%. As an illustration in Figure 13, the confidence interval bounds at 95% confidence level are shown for an arbitrary value of anomaly measure equal to 0.225 (lower bound=0.6610 and upper bound=0.8464). The estimate  $\hat{\tau}_e$  of the expended life fraction  $\tau_e$  can be obtained at the point of highest probability, i.e. the mean of the distribution. The other useful parameter is the *remaining life fraction* whose estimate  $\hat{\tau}_r$  is obtained at any instant as:  $\hat{\tau}_r = 1 - \hat{\tau}_e$ . The information on the remaining life estimate in a real-time experiment is useful for development of life extending control and resilient control strategies for prevention of widespread structural damage and catastrophic failures.

### 7.2.3. Experimental Validation and Results

The proposed methodology is validated by fatigue experiments on three new test specimens. The profiles of anomaly measure are computed using the *SDF* method for these three test specimens. Figure 13 also shows the profiles of the three test samples along with the plots of confidence interval bounds derived from the statistical ensemble. The estimates of the mean  $\hat{\tau}_e$  of the expended life fraction with the standard deviation  $\hat{\sigma}$  are obtained at (arbitrary) different values of the anomaly measure using the procedure described in the previous section. The results are interpolated for values of the anomaly measure that lie in between the two columns of the pattern matrix  $\mathcal{T}$ . Confidence interval bounds are obtained at three different confidence levels of 95%, 85% and 75%.

Figure 13 shows that the uncertainty in the fatigue damage is higher in the crack initiation phase as indicated by the width of confidence intervals for any particular value of the anomaly measure. Subsequently, upon onset of the crack propagation phase, the confidence intervals are significantly more tight than those in the crack initiation phase. This observation is explained by the fact that the uncertainty in the crack initiation phase depends on the random distribution of flaws in the specimen [69]. During this crack initiation phase, small cracks originate from the microstructural damage (eg. dislocations, voids and inclusions) at multiple sites in the entire body of the material structure causing a high uncertainty in fatigue damage behavior. These multiple small cracks eventually develop into a single large crack leading to the onset of crack propagation phase. Therefore, the uncertainty in the crack initiation phase relates to the inhomogeneity in the material and non-uniform distribution of the initial conditions in the specimen causing stress augmentation at certain locations which directly affects the formation of small cracks.

As such, the information that is derived during the crack initiation phase can act as an early warning of the onset of widespread fatigue in the crack propagation phase. The information from Figure 13 (including the estimate of  $\tau_e$  and different confidence intervals) can be utilized for real-time monitoring of the fatigue damage and for development of probabilistic robust control strategies for damage mitigation and prevention of catastrophic failures.

## 8. Summary, Conclusions and Recommendations for Future Work

### 8.1. Summary and Conclusions

The main contribution of this chapter is real-time monitoring of fatigue damage in polycrystalline alloys that are commonly used in mechanical structures. The chapter has demonstrated the capabilities of ultrasonic sensing technique for detection of small microstructural changes during early stages of fatigue damage. The chapter has adopted sensor based anomaly detection methodology because of the difficulty in achieving requisite accuracy in developing structural models of failure mechanisms at the microstructural level based on the fundamentals of physics. As such, an alternative approach is presented which relies on information based real time sensing of fatigue damage in mechanical systems.

This chapter presents a recently reported information-theoretic technique, called Sym-

bolic Dynamic Filtering (*SDF*), for real-time analysis of ultrasonic data. The underlying concept of *SDF* is built upon the principles of *Symbolic Dynamics*, *Information Theory*, and *Statistical Signal Processing*, where time series data from selected sensor(s) (e.g., ultrasonics) in the *fast* time scale of the process dynamics are analyzed at discrete epochs in the *slow* time scale of fatigue damage evolution. *SDF* includes pre-processing of ultrasonic data using the wavelet analysis, which is well suited for time-frequency analysis of non-stationary signals and enables noise attenuation from raw data. The wavelet-transformed data is partitioned using the maximum entropy principle to generate symbol sequences, such that the regions of data space with more information are partitioned finer and those with sparse information are partitioned coarser. Subsequently, robust statistical patterns of evolving damage are identified from these sequences by construction of a (probabilistic) finite-state machine that captures the dynamical system behavior by means of information compression.

Furthermore, the problem of fatigue damage monitoring is constructed into two sub-problems: (i) *Forward problem of Pattern Recognition* for characterization of the anomalous behavior, relative to the nominal behavior; and (ii) *Inverse problem of Pattern Identification* for estimation of parametric or non-parametric changes based on the knowledge assimilated in the forward problem and the observed time series data of quasi-stationary sensor measurements.

In this regard, this chapter has presented a statistical approach for estimation of the *remaining useful life*. To this effect, a stochastic data base of ultrasonic measurements has been generated from several experiments conducted under identical loading conditions. This data base has been analyzed to derive the behavioral pattern of fatigue damage under identical loading conditions which is subsequently used to provide the estimates of *used life fraction* in a fatigue experiment.

The codes of *SDF* are executable in real time and have been demonstrated in the laboratory environment for on-line monitoring of fatigue damage, based on the analysis of ultrasonic sensor signals, before any surface cracks are visible through the optical microscope in a special-purpose fatigue testing apparatus. In this research, the experiments have been conducted on the specimens fabricated from the aluminum alloy 7075-T6.

## 8.2. Recommendations for Future Work

The reported work is a step toward building a reliable instrumentation system for early detection of fatigue damage in polycrystalline alloys; further theoretical and experimental research is necessary before its usage in industry. While there are many research issues that need to be addressed, the following topics are being currently pursued and are recommended for future research:

1. *Investigation of other sensing techniques*- The research work reported in this chapter is based on an ultrasonic sensing technique. Future research would require investigation of the potential capabilities of other sensing techniques, such as acoustic emission, and eddy currents for early detection of fatigue damage and their real time implementation;
2. *Development of stochastic measures of fatigue crack growth in compact specimens*-

Future work requires development of stochastic models of fatigue crack damage under different loading conditions. Furthermore, the stochastic data bases crack growth can be used for studying complex phenomenon such as fractal behavior of fatigue damage evolution;

3. *Investigation of fatigue damage sensing under different loading conditions*- The results in this chapter are primary based on constant-amplitude low cycle loading conditions. Future work requires validation of the *SDF* technique for early detection of fatigue damage under different conditions, such as high-cycle loading, variable-amplitude loading, and spectral loading;
4. *Study of microstructural changes*- The work reported in this chapter is based on a dynamical data-driven approach that relies on ultrasonic sensing due to lack of accurate physics-based models during early stages of fatigue damage. Future work would require investigation of small microstructural changes during fatigue damage evolution. Analytical models of microstructural changes need to be formulated using advanced experimental devices such as the atomic force microscope and the scanning electron microscope;
5. *Investigation of surface deformities*- Future work requires to study the surface deformities occurring during the early stages of fatigue damage using the surface interferometer;
6. *Development of real time life extending control policies*- The information extracted from time series data using the *SDF* method can be used for development of control strategies for real time life extension and damage mitigation.

## Appendix A. Symbolic Dynamic Filtering Concept

This section presents a brief summary of the underlying concepts and essential features of a recently reported data-driven pattern identification tool called symbolic dynamic filtering (*SDF*) [21]. The concept of *SDF* is built upon the principles of several disciplines including *Symbolic Dynamics* [15, 20], *Statistical Pattern Recognition* [73], *Statistical Mechanics* [17], *Information Theory* [74] and *Probabilistic Finite State Machines* [16].

While the details are reported in recent publications [21, 22, 58, 17], the essential concepts of space partitioning, symbol sequence generation, construction of a finite-state machine from the generated symbol sequence and pattern recognition are consolidated here and succinctly described for self-sufficiency, completeness and clarity of the chapter.

### Appendix A.1. Symbolic Dynamic Encoding

The continuously-varying finite-dimensional model of a dynamical system is usually formulated in the setting of an initial value problem as:

$$\frac{d\mathbf{x}(t)}{dt} = f(\mathbf{x}(t), \theta(t_s)); \mathbf{x}(0) = \mathbf{x}_0, \quad (\text{A.1})$$

where  $t \in [0, \infty)$  denotes the (fast-scale) time;  $\mathbf{x} \in \mathbb{R}^n$  is the state vector in the phase space; and  $\theta \in \mathbb{R}^\ell$  is the (possibly anomalous) parameter vector varying in (slow-scale) time  $t_s$ . The gradual change in the parameter vector  $\theta \in \mathbb{R}^\ell$  due to possible evolution of anomalies can alter the system dynamics and hence change the state trajectory.

Let  $\Omega \subset \mathbb{R}^n$  be a compact (i.e., closed and bounded) region, within which the trajectory of the dynamical system, governed by Eq. (A.1), is circumscribed as illustrated in Fig. 8. The region  $\Omega$  is partitioned as  $\{\Phi_0, \dots, \Phi_{|\Sigma|-1}\}$  consisting of  $|\Sigma|$  mutually exclusive (i.e.,  $\Phi_j \cap \Phi_k = \emptyset \ \forall j \neq k$ ), and exhaustive (i.e.,  $\bigcup_{j=0}^{|\Sigma|-1} \Phi_j = \Omega$ ) cells, where  $\Sigma$  is the *symbol alphabet* that labels the partition cells. A trajectory of the dynamical system is described by the discrete time series data as:  $\{\mathbf{x}_0, \mathbf{x}_1, \mathbf{x}_2, \dots\}$ , where each  $\mathbf{x}_i \in \Omega$ . The trajectory passes through or touches one of the cells of the partition; accordingly the corresponding symbol is assigned to each point  $\mathbf{x}_i$  of the trajectory as defined by the mapping  $\mathcal{M} : \Omega \rightarrow \Sigma$ . Therefore, a sequence of symbols is generated from the trajectory starting from an initial state  $\mathbf{x}_0 \in \Omega$ , such that:

$$\mathbf{x}_0 \mapsto s_0 s_1 s_2 \dots s_j \dots \quad (\text{A.2})$$

where  $s_k \triangleq \mathcal{M}(\mathbf{x}_k)$  is the symbol generated at the (fast scale) instant  $k$ . The symbols  $s_k$ ,  $k = 0, 1, \dots$  are identified by an index set  $\mathcal{I} : \mathbb{Z} \rightarrow \{0, 1, 2, \dots, |\Sigma| - 1\}$ , i.e.,  $\mathcal{I}(k) = i_k$  and  $s_k = \sigma_{i_k}$  where  $\sigma_{i_k} \in \Sigma$ . Equivalently, Eq. (A.2) is expressed as:

$$\mathbf{x}_0 \mapsto \sigma_{i_0} \sigma_{i_1} \sigma_{i_2} \dots \sigma_{i_j} \dots \quad (\text{A.3})$$

The mapping in Eq. (A.2) and Eq. (A.3) is called *Symbolic Dynamics* as it attributes a legal (i.e., physically admissible) symbol sequence to the system dynamics starting from an initial state. The partition is called a generating partition of the phase space  $\Omega$  if every legal (i.e., physically admissible) symbol sequence uniquely determines a specific initial condition  $\mathbf{x}_0$ . In other words, every (semi-infinite) symbol sequence uniquely identifies one continuous space orbit [19].

Symbolic dynamics may also be viewed as coarse graining of the phase space, which is subjected to (possible) loss of information resulting from granular imprecision of partitioning boxes. However, the essential robust features (e.g., periodicity and chaotic behavior of an orbit) are expected to be preserved in the symbol sequences through an appropriate partitioning of the phase space [18].

Figure 8 pictorially elucidates the concepts of partitioning a finite region of the phase space and the mapping from the partitioned space into the symbol alphabet, where the symbols are indicated by Greek letters (e.g.,  $\alpha, \beta, \gamma, \delta, \dots$ ). This represents a spatial and temporal discretization of the system dynamics defined by the trajectories. Figure 8 also shows conversion of the symbol sequence into a finite-state machine and generation of the state probability vectors at the current and the reference conditions. The states of the finite state machine and the histograms in Fig. 8 are indicated by numerics (i.e., 1, 2, 3 and 4). Although the theory of phase-space partitioning is well developed for one-dimensional mappings [19], very few results are known for two and higher dimensional systems. Furthermore, the state trajectory of the system variables may be unknown in case of systems for which a model as in Eq. (A.1) is not known or is difficult to obtain. As such, as an alternative, the time series data set of selected observable outputs can be used for symbolic dynamic encoding as explained in the following subsection.

## Appendix A.2. Wavelet Space Partitioning

As described earlier, a crucial step in symbolic dynamic filtering (*SDF*) is partitioning of the phase space for symbol sequence generation [20]. Several partitioning techniques have been reported in literature for symbol generation [14][59], primarily based on symbolic false nearest neighbors (*SFNN*). These techniques rely on partitioning the phase space and may become cumbersome and extremely computation-intensive if the dimension of the phase space is large. Moreover, if the time series data is noise-corrupted, then the symbolic false neighbors would rapidly grow in number and require a large symbol alphabet to capture the pertinent information on the system dynamics. The wavelet transform [67] largely alleviates these shortcomings and is particularly effective with noisy data from high-dimensional dynamical systems [58]. As such, this chapter has used a wavelet-based partitioning approach [21][58] for construction of symbol sequences from time series data.

In wavelet-based partitioning approach, time series data are first converted to wavelet domain, where wavelet coefficients are generated at different time shifts. The choice of the wavelet basis function and wavelet scales depends on the time-frequency characteristics of individual signals. Guidelines for selection of basis functions and scales are reported in literature [58].

The wavelet space is partitioned with alphabet size  $|\Sigma|$  into segments of coefficients on the ordinate separated by horizontal lines. The choice of  $|\Sigma|$  depends on specific experiments, noise level and also the available computation power. A large *alphabet* may be noise-sensitive while a small alphabet could miss the details of signal dynamics [58]. The partitioning is done such that the regions with more information are partitioned finer and those with sparse information are partitioned coarser. This is achieved by maximizing the Shannon entropy [74], which is defined as:

$$S = - \sum_{i=0}^{|\Sigma|-1} p_i \log(p_i) \quad (\text{A.4})$$

where  $p_i$  is the probability of a data point to be in the  $i^{\text{th}}$  partition segment. Uniform probability distribution, i.e.,  $p_i = \frac{1}{|\Sigma|}$  for  $i = 0, 1, \dots, |\Sigma| - 1$ , is a consequence of maximum entropy partitioning [58]. Each partition segment is labelled by a symbol from the alphabet  $\Sigma$  and accordingly the symbol sequence is generated from the wavelet coefficients. The structure of the partition is fixed at the nominal condition, which serves as the reference frame for symbol sequence generation from time series data at anomalous condition(s).

Recently, an alternative method called Analytic Signal Space Partitioning (*ASSP*) [75] has been reported for symbolic time series analysis. The underlying concept of *ASSP* is built upon Hilbert transform of the real-valued data sequence into corresponding complex-valued analytic signal sequence that, in turn, is partitioned in the 2-dimensional plane.

## Appendix A.3. Probabilistic Finite State Machine (*PFSM*)

Once the symbol sequence is obtained, the next step is the construction of a Probabilistic Finite State Machine (*PFSM*) and calculation of the respective state probability vector as

depicted in the lower part of Fig. 8 by the histograms. The partitioning is performed at the nominal condition that is chosen to be the healthy state having no anomalies.

A *PFSM* is then constructed at the nominal condition, where the states of the machine are defined corresponding to a given *alphabet* set  $\Sigma$  and window length  $D$ . The alphabet size  $|\Sigma|$  is the total number of partition segments while the window length  $D$  is the length of consecutive symbol words [21], which are chosen as all possible words of length  $D$  from the symbol sequence. Each state belongs to an equivalence class of symbol words of length  $D$ , which is characterized by a word of length  $D$  at the leading edge. Therefore, the number  $n$  of such equivalence classes (i.e., states) is less than or equal to the total permutations of the alphabet symbols within words of length  $D$ . That is,  $n \leq |\Sigma|^D$ ; some of the states may be forbidden, i.e., these states have zero probability of occurrence. For example, if  $\Sigma = \{\alpha, \beta\}$ , i.e.,  $|\Sigma| = 2$  and if  $D = 2$ , then the number of states is  $n \leq |\Sigma|^D = 4$ ; and the possible states are words of length  $D = 2$ , i.e.,  $\alpha\alpha, \alpha\beta, \beta\alpha$ , and  $\beta\beta$ .

The choice of  $|\Sigma|$  and  $D$  depends on specific applications and the noise level in the time series data as well as on the available computation power and memory availability. As stated earlier, a large *alphabet* may be noise-sensitive and a small alphabet could miss the details of signal dynamics. Similarly, while a larger value of  $D$  is more sensitive to signal distortion, it would create a much larger number of states requiring more computation power and increased length of the data sets. Applications such as two-dimensional image processing, may require larger values of the parameter  $D$  and hence possibly larger number of states in the *PFSM*.

Using the symbol sequence generated from the time series data, the state machine is constructed on the principle of sliding block codes [15]. The window of length  $D$  on a symbol sequence is shifted to the right by one symbol, such that it retains the most recent  $(D-1)$  symbols of the previous state and appends it with the new symbol at the extreme right. The symbolic permutation in the current window gives rise to a new state. The *PFSM* constructed in this fashion is called the  $D$ -Markov machine [21], because of its Markov properties.

**Definition 1.1** *A symbolic stationary process is called  $D$ -Markov if the probability of the next symbol depends only on the previous  $D$  symbols, i.e.,  $P(s_j | s_{j-1} \dots s_{j-D} s_{j-D-1} \dots) = P(s_j | s_{j-1} \dots s_{j-D})$ .*

The finite state machine constructed above has  $D$ -Markov properties because the probability of occurrence of symbol  $\sigma \in \Sigma$  on a particular state depends only on the configuration of that state, i.e., the previous  $D$  symbols. The states of the machine are marked with the corresponding symbolic word permutation and the edges joining the states indicate the occurrence of a symbol  $\sigma$ . The occurrence of a symbol at a state may keep the machine in the same state or move it to a new state.

**Definition 1.2** *Let  $\Xi$  be the set of all states of the finite state machine. Then, the probability of occurrence of symbols that cause a transition from state  $\xi_j$  to state  $\xi_k$  under the mapping  $\delta : \Xi \times \Sigma \rightarrow \Xi$  is defined as:*

$$\pi_{jk} = P(\sigma \in \Sigma \mid \delta(\xi_j, \sigma) \rightarrow \xi_k); \sum_k \pi_{jk} = 1; \quad (\text{A.5})$$

Thus, for a  $D$ -Markov machine, the irreducible stochastic matrix  $\mathbf{\Pi} \equiv [\pi_{ij}]$  describes all transition probabilities between states such that it has at most  $|\Sigma|^{D+1}$  nonzero entries. The definition above is equivalent to an alternative representation such that,

$$\pi_{jk} \equiv P(\xi_k|\xi_j) = \frac{P(\xi_j, \xi_k)}{P(\xi_j)} = \frac{P(\sigma_{i_0} \cdots \sigma_{i_{D-1}} \sigma_{i_D})}{P(\sigma_{i_0} \cdots \sigma_{i_{D-1}})} \quad (\text{A.6})$$

where the corresponding states are denoted by  $\xi_j \equiv \sigma_{i_0} \cdots \sigma_{i_{D-1}}$  and  $\xi_k \equiv \sigma_{i_1} \cdots \sigma_{i_D}$ . This phenomenon is a consequence of the *PFSM* construction based on the principle of sliding block codes described above, where the occurrence of a new symbol causes a transition to another state or possibly the same state.

For computation of the state transition probabilities from a given symbol sequence at a particular slow time epoch, a  $D$ -block (i.e., a window of length  $D$ ) is moved by counting occurrences of symbol blocks  $\sigma_{i_0} \cdots \sigma_{i_{D-1}} \sigma_{i_D}$  and  $\sigma_{i_0} \cdots \sigma_{i_{D-1}}$ , which are respectively denoted by  $N(\sigma_{i_0} \cdots \sigma_{i_{D-1}} \sigma_{i_D})$  and  $N(\sigma_{i_0} \cdots \sigma_{i_{D-1}})$ . Note that if  $N(\sigma_{i_0} \cdots \sigma_{i_{D-1}}) = 0$ , then the state  $\sigma_{i_0} \cdots \sigma_{i_{D-1}} \in \Xi$  has zero probability of occurrence. For  $N(\sigma_{i_0} \cdots \sigma_{i_{D-1}}) \neq 0$ , the estimates of the transitions probabilities are then obtained by these frequency counts as follows:

$$\pi_{jk} \approx \frac{N(\sigma_{i_0} \cdots \sigma_{i_{D-1}} \sigma_{i_D})}{N(\sigma_{i_0} \cdots \sigma_{i_{D-1}})} \quad (\text{A.7})$$

where the criterion for convergence of the estimated  $\pi_{jk}$ , is given in [22] as a stopping rule for frequency counting.

The symbol sequence generated from the time series data at the nominal condition, set as a benchmark, is used to compute the *state transition matrix*  $\mathbf{\Pi}$  using Eq. (A.7). The left eigenvector  $\mathbf{p}$  corresponding to the unique unit eigenvalue of the irreducible stochastic matrix  $\mathbf{\Pi}$  is the probability vector whose elements are the stationary probabilities of the states belonging to  $\Xi$  [21][17]. The partitioning of time series data and the state machine structure should be the same in both nominal and anomalous cases but the respective state transition matrices could be different.

#### Appendix A.4. Pattern Identification Procedure

Behavioral pattern changes are quantified as deviations from the nominal behavior (i.e., the probability distribution at the nominal condition). The resulting anomalies (i.e., deviations of the evolving patterns from the nominal pattern) are characterized by a scalar-valued function, called *Anomaly Measure*  $\psi$  that is quasi-static in the fast time scale and is monotonically non-decreasing in the slow time scale. The state probability vector at any time instant corresponds to a singleton point on the unity-radius hypersphere. During fatigue damage evolution, the tip of the probability vector moves along a path on the surface of this hypersphere. The initial starting point of the path is the probability vector with uniform distribution obtained with maximum entropy partitioning (see Section Appendix A.2.). As the damage progresses, the probability distribution changes; eventually when a very large crack is formed, complete attenuation of the ultrasonic signal occurs and consequently the tip of the probability vector reaches a point where all states have zero probabilities of occurrence except one which has a probability one (i.e., a delta-distribution); this state corresponds to

the partition region where all data points are clustered due to complete attenuation of the signal.

In the context of fatigue damage, the anomaly measure is formulated on the following assumptions.

- *Assumption #1*: The damage evolution is an irreversible process (i.e., with zero probability of self healing) and implies the following conditions.

$$\psi^k \geq 0; \quad \psi^{k+\ell} - \psi^k \geq 0 \quad \forall \ell \geq 0 \quad \forall k \quad (\text{A.8})$$

- *Assumption #2*: The damage accumulation between two time epochs is a path function, i.e., dependent on the path traversed to reach the target state from the initial state.

In the context of fatigue damage in polycrystalline alloys at room temperature, the crack length is traditionally defined by a straight line joining the starting point to the tip of the crack but, in reality, the actual crack follows a complicated path (possibly fractal in ductile materials). In fact, at the initial stages of fatigue damage, there can be multiple short cracks oriented in different directions. Therefore, crack length alone does not provide complete information on fatigue damage evolution. Since ultrasonic signals are highly sensitive to small micro-structural changes, signal distortion is a good index of anomaly growth. The tip of the probability vector, obtained through symbolic dynamic filtering (*PDF*) method, moves along a curved path on the surface of the unity-radius hypersphere between the initial point  $\mathbf{p}^0$  (i.e., uniform distribution obtained under maximum entropy partitioning) and the final point at very large crack formation  $\mathbf{p}^f$  (i.e.,  $\delta$ -distribution due to complete attenuation of the signal). The phenomenon such as piling up of dislocations, strain hardening or reflections from multiple crack surfaces affect the ultrasonic signals in a variety of ways. An increase of the ultrasonic amplitude is also observed during very early stages of fatigue damage due to hardening of the material. On the other hand, ultrasonic signals attenuate sharply at the crack propagation stage upon development of a large crack.

As such, distortion of ultrasonic signals at a single time epoch may not uniquely determine the state of fatigue damage. The rationale is that two signals may exhibit similar characteristics but, in terms of actual incurred damage, the states are entirely different. Consequently, fatigue damage is a path function instead of being a state function. This assessment is consistent with assumption #1 implying that the damage evolution is irreversible. That is, at two different time epochs, the damage cannot be identical unless the net damage increment is zero. Consequently, by assumption #2, the anomaly measure should follow the traversed path of the probability vector, not the straight line joining the end points (i.e., the tips of the probability vectors).

The anomaly measure, based on the path between the nominal state to the completely damaged state, can be different even for identical test samples and under the same loading conditions because of the stochastic nature of fatigue phenomena. As such, analysis of a stochastic data set collected under identical experimental conditions is essential for identification of variations in different data sets. The following distance function is derived between probability vectors at two time epochs:

$$d(\mathbf{p}^k, \mathbf{p}^l) \equiv \sqrt{(\mathbf{p}^k - \mathbf{p}^l)^T (\mathbf{p}^k - \mathbf{p}^l)} \quad (\text{A.9})$$

The algorithm for computation of the anomaly measure  $\psi$  compensates for spurious measurement and computation noise in terms of the sup norm which is defined as  $\|\mathbf{e}\|_\infty \equiv \max(|e_1|, \dots, |e_m|)$  of the error in the probability vector (i.e., the maximum error in the elements of the probability vector). The algorithm is presented below.

- i)  $\psi^0 = 0; \delta\psi^1 = 0; \tilde{\mathbf{p}} = \mathbf{p}^0; k = 1;$
- ii) if  $\|\mathbf{p}^k - \tilde{\mathbf{p}}\|_\infty > \epsilon$  then  $\delta\psi^k = d(\mathbf{p}^k, \tilde{\mathbf{p}})$  and  $\tilde{\mathbf{p}} \leftarrow \mathbf{p}^k;$
- iii)  $\psi^k = \psi^{k-1} + \delta\psi^k;$
- iv)  $k \leftarrow k + 1; \delta\psi^k = 0;$  go to step (ii).

The real positive parameter  $\epsilon$ , is associated with the robustness of the measure against measurement and computation noise and is identified by performing an experiment with a sample with no notch. Since there is no notch there is practically no stress augmentation and relatively no fatigue damage. As such, the parameter  $\epsilon$  is estimated as:

$$\epsilon \approx \max_{l \in \{1, \dots, N\}} (\|\mathbf{p}^{l+1} - \mathbf{p}^l\|_\infty) \quad (\text{A.10})$$

from  $N$  consecutive observations with  $N \gg 1$ .

The algorithm works in the following fashion: the reference point  $\tilde{\mathbf{p}}$  is initialized to the starting point  $\mathbf{p}^0$  and anomaly measure  $\psi^0$  is set to 0. At any slow time epoch  $t_k$  if the state probability vector moves such that the distance travelled in any particular direction (i.e. the sup norm  $\|\bullet\|_\infty$ ) is greater than  $\epsilon$  as specified in step (ii), then the anomaly measure is incremented by  $\delta\psi^k = d(\mathbf{p}^k, \tilde{\mathbf{p}})$  and the reference point is shifted to the current point  $\mathbf{p}^k$ . The procedure is repeated at all slow time epochs. As such, the total path travelled by the tip of probability vector represents the deviation from the nominal condition and the associated damage.

### Appendix A.5. Summary of *SDF*-based Pattern Recognition

The symbolic dynamic filtering (*SDF*) method of statistical pattern recognition for anomaly detection is summarized below.

- Acquisition of time series data from appropriate sensor(s) variables at a nominal condition, when the system is assumed to be in the healthy state (i.e., zero anomaly measure)
- Generation of the wavelet transform coefficients of the data obtained with an appropriate choice of the wavelet basis and scale [58]
- Maximum entropy partitioning in the wavelet domain at the nominal condition (see Appendix A.2.) and generation of the corresponding symbol sequence
- Construction of the *D*-Markov machine and computation of the state probability vector  $\mathbf{p}^0$  at the nominal condition

- Generation of a time series data sequence at another (possibly) anomalous condition and conversion to the wavelet domain to generate the respective symbolic sequence based on the partitioning constructed at the nominal condition
- Computation of the corresponding state probability vector  $\mathbf{p}$  using the finite state machine constructed at the nominal condition
- Computation of scalar *anomaly measure*  $\mu$ .

Capability of *SDF* has been demonstrated for anomaly detection at early stages of gradually evolving anomalies by real-time experimental validation. In this regard, major advantages of *SDF* are listed below:

- i. Robustness to measurement noise and spurious signals [58]
- ii. Adaptability to low-resolution sensing due to the coarse graining in space partitions [21]
- iii. Capability for small change detection because of sensitivity to signal distortion [44] and
- iv. Real-time execution on commercially available inexpensive platforms [62][44].

### Appendix A.6. Stopping Rule for Determining Symbol Sequence Length

This appendix presents a stopping rule that is necessary to find a lower bound on the length of symbol sequence required for parameter identification of the stochastic matrix  $\mathbf{\Pi}$ . The stopping rule [22] is based on the properties of irreducible stochastic matrices [76]. The state transition matrix, constructed at the  $r^{th}$  iteration (i.e., from a symbol sequence of length  $r$ ), is denoted as  $\mathbf{\Pi}(r)$  that is an  $n \times n$  irreducible stochastic matrix under stationary conditions. Similarly, the state probability vector  $\mathbf{p}(r) \equiv [p_1(r) \ p_2(r) \ \cdots \ p_n(r)]$  is obtained as

$$p_i(r) = \frac{r_i}{\sum_{j=1}^n r_j} \quad (\text{A.11})$$

where  $r_i$  is the number of  $D$ -blocks (i.e., symbol strings of length  $D$ ) representing the  $i^{th}$  state such that  $(\sum_{j=1}^n r_j) + D - 1 = r$  is the total length of the data sequence under symbolization. The stopping rule makes use of the Perron-Frobenius Theorem [76] to establish a relation between the vector  $\mathbf{p}(r)$  and the matrix  $\mathbf{\Pi}(r)$ . Since the matrix  $\mathbf{\Pi}(r)$  is stochastic and irreducible, there exists a unique eigenvalue  $\lambda = 1$  and the corresponding left eigenvector  $\mathbf{p}(r)$  (normalized to unity in the sense of absolute sum). The left eigenvector  $\mathbf{p}(r)$  represents the state probability vector, provided that the matrix parameters have converged after a sufficiently large number of iterations. That is, under the hypothetical arbitrarily long sequences, the following condition is assumed to hold.

$$\mathbf{p}(r+1) = \mathbf{p}(r)\mathbf{\Pi}(r) \Rightarrow \mathbf{p}(r) = \mathbf{p}(r)\mathbf{\Pi}(r) \text{ as } r \rightarrow \infty \quad (\text{A.12})$$

Following Eq. (A.11), the absolute error between successive iterations is obtained such that

$$\| (\mathbf{p}(r) - \mathbf{p}(r+1)) \|_{\infty} = \| \mathbf{p}(r) (\mathbf{I} - \mathbf{\Pi}(r)) \|_{\infty} \leq \frac{1}{r} \quad (\text{A.13})$$

where  $\| \bullet \|_{\infty}$  is the max norm of the finite-dimensional vector  $\bullet$ .

To calculate the stopping point  $r_{stop}$ , a tolerance of  $\eta$  ( $0 < \eta \ll 1$ ) is specified for the relative error such that:

$$\frac{\| (\mathbf{p}(r) - \mathbf{p}(r+1)) \|_{\infty}}{\| (\mathbf{p}(r)) \|_{\infty}} \leq \eta \quad \forall r \geq r_{stop} \quad (\text{A.14})$$

The objective is to obtain the least conservative estimate for  $r_{stop}$  such that the dominant elements of the probability vector have smaller relative errors than the remaining elements. Since the minimum possible value of  $\| (\mathbf{p}(r)) \|_{\infty}$  for all  $r$  is  $\frac{1}{n}$ , where  $n$  is the dimension of  $\mathbf{p}(r)$ , the least of most conservative values of the stopping point is obtained from Eqs. (A.13) and (A.14) as:

$$r_{stop} \equiv \text{int} \left( \frac{n}{\eta} \right) \quad (\text{A.15})$$

where  $\text{int}(\bullet)$  is the integer part of the real number  $\bullet$ .

## References

- [1] S. Ozekici, *Reliability and Maintenance of Complex Systems*, vol. 154. NATO Advanced Science Institutes (ASI) Series F: Computer and Systems Sciences, Berlin, Germany, 1996.
- [2] E. E. Keller and A. Ray, "Real time health monitoring of mechanical structures," *Structural Health Monitoring*, vol. 2(3), pp. 191–203, 2003.
- [3] M. A. Meggiolaro and J. T. P. Castro, "Statistical evaluation of strain-life fatigue crack initiation predictions," *International Journal of Fatigue*, vol. 26, pp. 463–476, 2004.
- [4] P. Johannesson, T. Svensson, and M. D. Jacques, "Fatigue life prediction based on variable amplitude tests-methodology," *International Journal of Fatigue*, vol. 27, pp. 954–965, 2005.
- [5] S. Ishihara and A. J. McEvily, "Analysis of short fatigue crack growth in cast aluminium alloys," *International Journal of Fatigue*, vol. 24, pp. 1169–1174, 2002.
- [6] C. Bjerken and S. Melin, "A tool to model short crack fatigue growth using a discrete dislocation formulation," *International Journal of Fatigue*, vol. 25, pp. 559–566, 2003.
- [7] M. D. Chapetti, "Fatigue propagation threshold for short cracks under constant amplitude loading," *International Journal of Fatigue*, vol. 25, pp. 1319–1326, 2003.
- [8] D. V. Ramsamooj, "Analytical prediction of short to long fatigue crack growth rate using small- and large-scale yielding fracture mechanics," *International Journal of Fatigue*, vol. 25, pp. 923–933, 2003.

- 
- [9] R. K. Pathria, *Statistical Mechanics*. Elsevier Science and Technology Books, 1996.
- [10] E. Ott., *Chaos in Dynamical Systems*. Cambridge University Press, 1993.
- [11] K. Sobczyk and B. F. Spencer, *Random Fatigue: Data to Theory*. Academic Press, Boston, MA, 1992.
- [12] N. Scafetta, A. Ray, and B. J. West, “Correlation regimes in fluctuations of fatigue crack growth,” *Physica A*, vol. 59, no. 3.
- [13] A. Ray, “Stochastic measure of fatigue crack damage for health monitoring of ductile alloy structures,” *Structural Health Monitoring*, vol. 3, no. 3, pp. 245–263, 2004.
- [14] H. Kantz and T. Schreiber, *Nonlinear Time Series Analysis, 2nd ed.* Cambridge University Press, United Kingdom, 2004.
- [15] D. Lind and M. Marcus, *An Introduction to Symbolic Dynamics and Coding*. Cambridge University Press, United Kingdom, 1995.
- [16] H. E. Hopcroft, R. Motwani, and J. D. Ullman, *Introduction to Automata Theory, Languages, and Computation, 2nd ed.* Addison Wesley, Boston, 2001.
- [17] S. Gupta and A. Ray, “Statistical mechanics of complex systems for pattern identification,” *Journal of Statistical Physics*, vol. 134, no. 2, pp. 337–364, 2009.
- [18] R. Badii and A. Politi, *Complexity hierarchical structures and scaling in physics*. Cambridge University Press, United Kingdom, 1997.
- [19] C. Beck and F. Schlögl, *Thermodynamics of chaotic systems: an introduction*. Cambridge University Press, United Kingdom, 1993.
- [20] C. S. Daw, C. E. A. Finney, and E. R. Tracy, “A review of symbolic analysis of experimental data,” *Review of Scientific Instruments*, vol. 74, no. 2, pp. 915–930, 2003.
- [21] A. Ray, “Symbolic dynamic analysis of complex systems for anomaly detection,” *Signal Processing*, vol. 84, no. 7, pp. 1115–1130, 2004.
- [22] S. Gupta and A. Ray, *Symbolic Dynamic Filtering for Data-Driven Pattern Recognition, Chapter 2 in Pattern Recognition: Theory and Application*. Nova Science Publisher, Hauppauge, New York, Editor- Erwin A. Zoeller, 2007.
- [23] S. Gupta and A. Ray, “Pattern identification using lattice spin systems: A thermodynamic formalism,” *Applied Physics Letters*, vol. 91, no. 19, p. 194105, 2007.
- [24] S. Grondel, C. Delebarre, J. Assaad, J. P. Dupuis, and L. Reithler, “Fatigue crack monitoring of riveted aluminium strap joints by lamb wave analysis and acoustic emission measurement techniques,” *NDT&E international*, vol. 35, pp. 339–351, 2006.
- [25] D. A. Cook and Y. H. Berthelot, “Detection of small surface-breaking fatigue cracks in steel using scattering of rayleigh waves,” *NDT&E international*, vol. 34, pp. 483–492, 2001.

- [26] V. Zilberstein, K. Walrath, D. Grundy, D. Schlicker, N. Goldfine, E. Abramovici, and T. Yentzer, "Mwm eddy-current arrays for crack initiation and growth monitoring," *International Journal of Fatigue*, vol. 25, pp. 1147–1155, 2003.
- [27] A. Witney, Y. F. Li, J. Wang, M. Z. Wang, J. J. DeLuccia, and C. Laird, "Electrochemical fatigue sensor response to ti-6wt% al-4wt% v and 4130 steel," *Philosophical Magazine*, vol. 84, no. 3-5, pp. 331–349, 2004.
- [28] B. Yang, P. K. Liaw, G. Wang, W. H. Peter, R. Buchanan, Y. Yokoyama, J. Y. Huang, R. C. Kuo, J. G. Huang, D. E. Fielden, and D. L. Klarstrom, "Thermal-imaging technologies for detecting damage during high-cycle fatigue," *Metallurgical and Materials Transactions A*, vol. 35A, pp. 15–24, 2004.
- [29] S. W. Doebling, C. R. Farrar, and M. B. Prime, "A summary review of vibration-based damage identification methods," *The Shock and Vibration Digest*, vol. 30, no. 2, pp. 91–105, 1998.
- [30] A. Almeida and E. V. K. Hill, "Neural network detection of fatigue crack growth in reveted joints using acoustic emission," *Mat. Eval.*, vol. 53, no. 1, pp. 76–82, 1995.
- [31] J. Baram, "Fatigue-life prediction by an order statistics treatment of acoustic-emission signals," *Exper. Mech.*, vol. 33, pp. 189–194, 1993.
- [32] M. N. Bassim, S. S. Lawrence, and C. D. Liu, "Detection of the onset of fatigue crack growth in rail steels using acoustic emission," *Eng. Fracture Mech.*, vol. 47, no. 2, pp. 207–214, 1994.
- [33] D. O. Harris and H. L. Dunegan, "Continuous monitoring of fatigue-crack growth by acoustic-emission techniques," *Exper. Mech.*, vol. 14, pp. 71–80, 1974.
- [34] K. Y. Lee, "Cyclic ae count rate and crack growth rate under low cycle fatigue fracture loading," *Eng. Fracture Mech.*, vol. 34, no. 5/6, pp. 1069–1073, 1989.
- [35] M. V. Lysak, "Development of the theory of acoustic emission by propagating cracks in terms of fracture mechanics," *Eng. Fracture Mech.*, vol. 55, no. 3, pp. 443–452, 1996.
- [36] M. Scala and S. M. Cousland, "Acoustic emission during fatigue crack propagation in the aluminium alloys 2024 and 2124," *Mat. Sci. and Eng.*, vol. 61, pp. 211–218, 1983.
- [37] V. Zilberstein, D. Grundy, V. Weiss, N. Goldfine, E. Abramovici, J. Newman, and T. Yentzer, "Early detection and monitoring of fatigue in high strength steels with mwm-arrays," *International Journal of Fatigue*, vol. 27, pp. 1644–1652, 2005.
- [38] H. S. Bai, L. Y. Yu, and J. W. He (Ho), "A monitoring system for contact fatigue crack testing," *NDT International*, vol. 22, no. 3, pp. 162–167, 1989.
- [39] N. Yusa, L. Janousek, M. Rebican, Z. Chen, K. Miya, N. Chigusa, and H. Ito, "Detection of embedded fatigue cracks in inconel weld overlay and the evaluation of the minimum thickness of the weld overlay using eddy current testing," *Nuclear Engineering and Design*, vol. 236, no. 18, pp. 1852–1859, 2006.

- 
- [40] L. W. Anson, R. C. Chivers, and K. E. Puttick, "On the feasibility of detecting pre-cracking fatigue damage in metal matrix composites by ultrasonic techniques," *Composites science and technology*, vol. 55, pp. 63–73, 1995.
- [41] S. Vanlanduit, P. Guillaume, and G. V. D. Linden, "Online monitoring of fatigue cracks using ultrasonic surface waves," *NDT&E international*, vol. 36, pp. 601–607, 2003.
- [42] S. I. Rokhlin and J. Y. Kim, "In situ ultrasonic monitoring of surface fatigue crack initiation and growth from surface cavity," *International journal of fatigue*, vol. 25, pp. 41–49, 2003.
- [43] S. Kenderian, T. P. Berndt, R. E. Green, and B. B. Djordjevic, "Ultrasonic monitoring of dislocations during fatigue of pearlitic rail steel," *Material Science and Engineering*, vol. 348, pp. 90–99, 2003.
- [44] S. Gupta, A. Ray, and E. Keller, "Symbolic time series analysis of ultrasonic data for early detection of fatigue damage," *Mechanical Systems and Signal Processing*, vol. 21, no. 2, pp. 866–884, 2007.
- [45] S. Gupta, A. Ray, and E. Keller, "Online fatigue damage monitoring by ultrasonic measurements: A symbolic dynamics approach," *International Journal of Fatigue*, vol. 29, no. 6, pp. 1100–1114, 2007.
- [46] S. Gupta and A. Ray, "Real-time fatigue life estimation in mechanical systems," *Measurement Science and Technology*, vol. 18, no. 7, pp. 1947–1957, 2007.
- [47] E. E. Keller, *Real time sensing of fatigue crack damage for information-based decision and control*. PhD thesis, Department of Mechanical Engineering, Pennsylvania State University, State College, PA, 2001.
- [48] M. T. Resch and D. V. Nelson, "An ultrasonic method for measurement of size and opening behavior of small fatigue cracks," *Small-Crack Test Methods, ASTM STP 1149, J.M. Larsen and J.E. Allison, Eds., American Society for Testing and Materials, Philadelphia*, pp. 169–196, 1992.
- [49] P. B. Nagy, "Fatigue damage assessment by nonlinear ultrasonic materials characterization," *Ultrasonics*, vol. 36, pp. 375–381, 1998.
- [50] J. H. Cantrell and W. T. Yost, "Nonlinear ultrasonic characterization of fatigue microstructures," *International Journal of fatigue*, vol. 23, pp. 487–490, 2001.
- [51] J. L. Rose, *Ultrasonic waves in solid media*. Cambridge university press, 2004.
- [52] H. Sohn, C. R. Farrar, N. F. Hunter, and K. Wordan, "Structural health monitoring using statistical pattern recognition techniques," *Journal of Dynamic Systems, Measurement and Control*, vol. 123, pp. 706–711, December 2001.
- [53] Z. K. Peng and F. L. Chu, "Application of the wavelet transform in machine condition monitoring and fault diagnosis: a review with bibliography," *Mechanical Systems and Signal Processing*, vol. 18, pp. 199–221, 2004.

- 
- [54] X. Lou and K. A. Loparo, "Bearing fault diagnosis based on wavelet transform and fuzzy interference," *Mechanical Systems and Signal Processing*, vol. 18, pp. 1077–1095, 2004.
- [55] J. M. Nichols, M. D. Todd, M. Seaver, and L. N. Virgin, "Use of chaotic excitation and attractor property analysis in structural health monitoring," *Physical Review E*, vol. 67, no. 016209, 2003.
- [56] W. J. Wang, J. Chen, X. K. Wu, and Z. T. Wu, "The application of some non-linear methods in rotating machinery fault diagnosis," *Mechanical Systems and Signal Processing*, vol. 15, no. 4, pp. 697–705, 2001.
- [57] L. Moniz, J. M. Nichols, C. J. Nichols, M. Seaver, S. T. Trickey, M. D. Todd, L. M. Pecora, and L. N. Virgin, "A multivariate, attractor-based approach to structural health monitoring," *Journal of Sound and Vibration*, vol. 283, pp. 295–310, 2005.
- [58] V. Rajagopalan and A. Ray, "Symbolic time series analysis via wavelet-based partitioning," *Signal Processing*, vol. 86, no. 11, pp. 3309–3320, 2006.
- [59] M. Buhl and M. Kennel, "Statistically relaxing to generating partitions for observed time-series data," *Physical Review E*, vol. 71, no. 4, p. 046213, 2005.
- [60] J. P. Crutchfield and K. Young, "Inferring statistical complexity," *Physical Review Letters*, vol. 63, pp. 105–108, 1989.
- [61] J. P. Crutchfield, "The calculi of emergence: Computation dynamics and induction," *Physica*, vol. D, no. 75, pp. 11–54, 1994.
- [62] C. Rao, A. Ray, S. Sarkar, and M. Yasar, "Review and comparative evaluation of symbolic dynamic filtering for detection of anomaly patterns," *Signal, Image and Video Processing*, DOI 10.1007/s11760-008-0061-8, 2008.
- [63] A. Khatkhate, S. Gupta, A. Ray, and E. Keller, "Life extending control of mechanical structures using symbolic time series analysis," in *American Control Conference*, (Minnesota, USA), 2006.
- [64] A. Tarantola, *Inverse Problem Theory*. Society for Industrial and Applied Mathematics, 2005.
- [65] S. Suresh, *Fatigue of Materials*. Cambridge University Press, Cambridge, U.K., 1998.
- [66] *MATLAB Wavelet Toolbox*. Mathworks Inc, 2006.
- [67] S. Mallat, *A Wavelet Tour of Signal Processing 2/e*. Academic Press, 1998.
- [68] S. Gupta, *Behavioral Pattern Identification for Structural Health Monitoring in Complex Systems*. PhD thesis, Department of Mechanical Engineering, Pennsylvania State University, State College, PA, 2006.
- [69] M. Klesnil and P. Lukas, *Fatigue of Metallic Materials*. Material Science Monographs 71, Elsevier, 1991.

- [70] J. L. Bogdanoff and F. Kozin, *Probabilistic models of cumulative damage*. John Wiley, New York, 1985.
- [71] H. D. Brunk, *An introduction to mathematical statistics, 3rd Edn.* Xerox Publishing, Lexington, MA., 1995.
- [72] G. W. Snedecor and W. G. Cochran, *Statistical Methods*. Eighth Edition, Iowa State University, Press, 1989.
- [73] R. Duda, P. Hart, and D. Stork, *Pattern Classification*. John Wiley & Sons Inc., 2001.
- [74] T. M. Cover and J. A. Thomas, *Elements of Information Theory*. John Wiley, New York, 1991.
- [75] A. Subbu and A. Ray, "Space partitioning via hilbert transform for symbolic time series analysis," *Applied Physics Letters*, vol. 92, p. 084107, February 2008.
- [76] R. B. Bapat and T. E. S. Raghavan, *Nonnegative Matrices and Applications*. Cambridge University Press, 1997.